A Survey of Dense Multipath and Its Impact on Wireless Systems

Jiang, Suying; Wang, Wei; Miao, Yang ; Fan, Wei; Molisch, Andreas

Published in:
IEEE Open Journal of Antennas and Propagation

DOI (link to publication from Publisher):
10.1109/OJAP.2022.3168400

Publication date:
2022

Document Version
Publisher's PDF, also known as Version of record

Received 28 January 2022; revised 23 February 2022; accepted 23 February 2022. Date of publication 19 April 2022; date of current version 28 April 2022.

Digital Object Identifier 10.1109/OJAP.2022.3168400

A Survey of Dense Multipath and Its Impact on Wireless Systems

SUYING JIANG[1], WEI WANG[1] (Member, IEEE), YANG MIAO[2,3] (Member, IEEE), WEI FAN[4] (Senior Member, IEEE), AND ANDREAS F. MOLISCH[5] (Fellow, IEEE)

[1]School of Information Engineering, Chang'an University, Xi'an 710064, China

[2]Faculty of Electrical Engineering, University of Twente, 7500 AE Enschede, The Netherlands

[3]Faculty of Electrical Engineering, Katholieke Universiteit Leuven, 3000 Leuven, Belgium

[4]Department of Electronic Systems, Aalborg University, 9220 Aalborg, Denmark

[5]Department of Electrical and Computer Engineering, University of Southern California, Los Angeles, CA 90089, USA

CORRESPONDING AUTHOR: W. WANG (e-mail: wei.wang@chd.edu.cn)

This work was supported in part by the National Key Research and Development Program of China under Grant 2020YFB1807001, and in part by the National Natural Science Foundation of China under Grant 61871059. The work of Andreas F. Molisch was supported by the National Science Foundation under Grant CIF-1618078, Grant ECCS-1731694, and Grant ECCS-1926913.

ABSTRACT In recent years wireless propagation channel research has paid considerable attention to dense multipath, which is an indispensable part of propagation channels and may significantly contribute to the received power in variety of environments and frequency bands. Mathematical representation of dense multipath is different from that of specular components (SCs) due to its distinct propagation mechanism and impact on system performance. Therefore, accurate understanding and modeling of dense multipath together with SCs are important for parametric channel estimation and for reliable simulation in wireless applications. This paper first presents a systematic survey of studies of dense multipath in terms of different representations, channel modeling approaches and estimation methods. Thereafter, a comprehensive review of the characteristics and impact of dense multipath on performance of communication, localization and sensing systems is provided. Finally, open research topics are discussed.

INDEX TERMS Channel estimation, channel modeling, characteristics, communication, dense multipath.

I. INTRODUCTION

RADIO propagation channel modeling plays a significant role in designing and testing modern wireless systems for communications, localization, as well as sensing. Accurate models of wireless propagation channels provide not only fundamental performance limits, but also benefit the development of transceiver algorithms.

The requirements for channel models differ, depending on the environment, system parameters (e.g., bandwidth), and even the application. For example, channel models developed for terrestrial mobile radio systems normally are designed for communication applications and do not fulfill all requirements in the context of localization and sensing. Thus, as new systems, applications, and operating environments emerge, channel models need to be refined or modified.

Wireless propagation channels are commonly modeled by assuming that the emitted radio signal propagates to the receiver via several deterministic paths [1]–[3]. These deterministic paths are interpreted as specular components (SCs), i.e., dominant contributions of radio waves propagating from the transmitter (Tx) to the receiver (Rx), and arise, e.g., from reflection of a wave on a large smooth surface. However, it is insufficient to consider only SCs since radio wave propagation is more complex in reality. SCs are usually accompanied by numerous weak multipath components originated from the objects with sizes on the order of wavelengths or with macroscopic surface roughness, multi-bounce volume scattering, and scattering from curved surfaces. Therefore, it is difficult to represent all these propagation phenomena using the framework of SCs. This may introduce mismatch in signal model and, thus, inaccurate parametric channel estimates and modeling.

The part of the channel that cannot be resolved as SCs is usually referred to as the dense multipath component (DMC) [4]. Some studies showed that DMC has an important influence on the performance of communication system, such as the channel capacity [5], the channel estimation accuracy [6], the channel interpolation and extrapolation [7], etc. In [5], it was shown that diffuse scattering (DS) has negative impact on the multi-user multiple-input multiple-output (MIMO) capacity in the line-of-sight (LoS) scenarios, but DS has positive impact on the multi-user MIMO capacity in the non-line-of-sight (NLoS) scenarios. The impact of DMC on the SC parameters estimation accuracy was studied in [6]. Simulation results showed that the presence of DMC could strongly corrupt the Estimation of Signal Parameters via Rotational Invariant Techniques (ESPRIT) and space-alternating generalized expectation-maximization (SAGE) algorithms' ability to separate the signal subspace from the noise subspace, leading to a poor estimation accuracy of ESPRIT and SAGE. In [7], it is showed that DMC will lead to the performance degradation of frequency interpolation.

The contribution of DMC to the total received power strongly depends on the propagation environment, the distance and the frequency used. The DMC to total power ratio is significant in rich-multipath environments like indoors [8]–[10], industrial environments [11], [12] and urban areas [13], [14], where there exists a large number of DS propagation paths caused by irregular surfaces or volumes. Therefore, it leads to the fact that DMC must be considered both for accurate channel models [11], for parametric channel parameter estimations [15], [16], and for the design of communication systems.

Accurate overall channel models, which require accurate representation and modeling of DMC, are vital for obtaining accurate overall models of the propagation channels, as those can further assist the design and simulation of reliable and efficient wireless systems. In the development of these models, it is often required to consider the following aspects:

- proper generic representation and modeling of the DMC;
- accurate estimation of DMC from observations with limited bandwidth;
- characterization and parameterization of DMC.

In the past decades, different approaches to model DMC have been proposed, such as the joint angular delay power spectrum using an exponential decay in delay and the von Mises distribution (VMD) model in angle [14], [17]–[21], the multichannel autoregressive (MAR) model [22], autoregressive moving average model [23], deterministic models (e.g., ray tracing (RT)) [24], hybrid models [25], etc. In addition, some researchers modeled the DMC using the effective roughness (ER) models, the propagation graph (PG) models, etc. Depending on individual modeling approaches, different parameter estimation methods for DMC were proposed in previous works, such as the Richter's maximum-likelihood estimation method (RiMAX) [4], [26], the extended Kalman filter (EKF) [27], the autoregressive approach incorporated within the maximum likelihood (ML) based method of SAGE [22], or within the tracking method of Kalman enhanced super resolution tracking (KEST) [28]. There are also numerous studies focusing on the characteristics and parameterization of the DMC in the time-delay-angular domains.

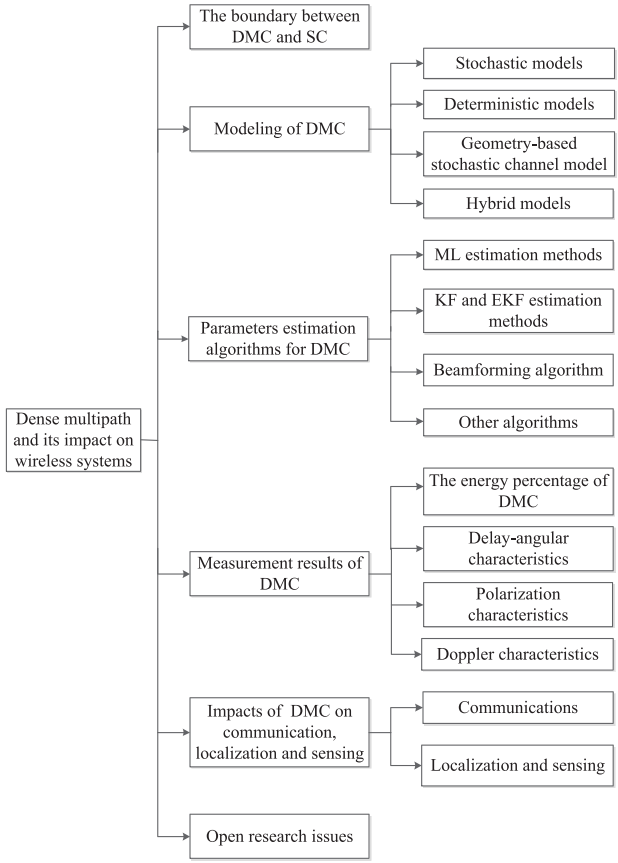

FIGURE 1. A flow chart of dense multipath and its impact on wireless systems.

Further, there has been significant interest in the influence of DMC on the performance of wireless applications like communications, localization and sensing. For either of those cases, accurate information and model of DMC are important to enhance the system performance and, thus, indispensable while developing and testing algorithms.

Despite this wealth of results that have been obtained over the past year, there is still a lack of a comprehensive survey for DMC that can help researchers to assess the available state of the art, and facilitate the development of future theory and measurements. Given the importance of the topic for the development of future wireless systems, this paper aims to fill this gap. In this paper, as shown in Fig. 1, we summarize recent results about modeling, parameter estimation, characterization and parameterization of DMC. Further, we also present a discussion of the impact of DMC on the performance of wireless communication, localization and

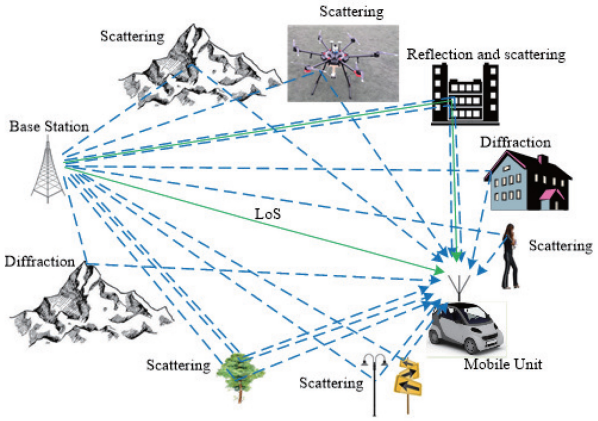

FIGURE 2. A typical scenario of multipath propagation for mobile communication.

sensing systems. Finally, we provide some open research issues on DMC.

The structure of this paper is as follows: In Section II, we discuss the distinctions between SC and DMC. In Section III, we give an overview of DMC modeling. The channel estimation methods for DMC are presented in Section IV. Measurements results are surveyed in Section V. The impact of DMC on communication, localization and sensing are presented in Section VI. Open research topics are outlined in Section VII. Finally, conclusions are drawn in Section VIII.

II. DISTINGUISHING BETWEEN DMC AND SC

A. DESCRIPTION OF DMC

In any wireless link, the signal received by the Rx is a superposition of multiple echoes of the transmitted signal, commonly called multipath components (MPCs). Fig. 2 visualizes an examplary multipath propagation scenario in an outdoor environment. There exists different propagation phenomena such as scattering by trees and rocks, reflection by the house facade and diffraction at the edge of objects [1]. The strong component reflected by the house facade can be described as SC, i.e., a specular-like propagation path. The scattered paths represented by dotted lines in Fig. 2 are originated from leaves, rough surfaces, traffic signs, lamp posts (curved metallic surface), etc.; these paths can be regarded as DMC. In fact, the SC like the reflected path by the house facade is usually accompanied by a DMC due to the surface irregularity of the facade.

B. DMC VS SC: WHERE IS THE BOUNDARY?

As the above example shows, channel descriptions incorporating the DMC can split the channel into contributions arising from the SCs, and contributions from the DMC. It is thus a fundamental question how to discriminate between those two types of contributions. This subsection will discuss this question from multiple perspectives. The main conclusion is that theoretically "clean" definitions have no equivalent practical meaning, so that only a heuristic definition that depends on the circumstances of the measurement or deployment conditions can be meaningfully done.

Let us first consider a mathematical representation. The wireless channel is generally described by the *double-directional impulse response* ,[1] which is typically modeled as a sum of MPCs that each represents a plane wave [30]

$$h(t, \tau, \Omega, \psi) = \sum_{\ell=1}^{N} h_\ell(t, \tau, \Omega, \psi), \tag{1}$$

where we denote the delay τ, the number of MPCs N, the *direction-of-departure (DOD)* Ω, $\Omega = [\varphi, \nu]$, where φ is the azimuth angle, ν is the elevation angle, the *direction-of-arrival (DOA)* ψ, $\psi = [\varphi, \nu]$. The $h_\ell(t, \tau, \Omega, \psi)$ is the contribution of the ℓ-th multipath component, modeled as

$$h_\ell(t, \tau, \Omega, \psi) = |a_\ell| e^{j\phi_\ell} \delta(\tau - \tau_\ell)\delta(\Omega - \Omega_\ell)\delta(\psi - \psi_\ell), \tag{2}$$

where a_ℓ and ϕ_ℓ are absolute amplitude and phase of the ℓ-th MPC, respectively. Such an expansion into a set of plane waves can represent any arbitrary field *if we allow* $N \to \infty$. Conversely, we can say that there can be at most a finite number of MPCs that have finite power, and are thus represented as Dirac delta functions in the above equation, while the DMC is described by an infinite number of components with infinitesimally small power each, or, in other words, by a continuous function in at least one of the domains τ, Ω, ψ. A DMC arises essentially from a model mismatch between the "*finite* sum of plane waves" assumption and the reality of complex propagation processes that include diffraction, and DS. A distinction between SC and DMC can be made by separating the MPCs with delta functions and finite amplitude, and the continuous remainder.

Such a purely mathematical definition seems straightforward, but has some major pitfalls. Firstly, in order to identify SCs with a perfect $\delta(\tau)$, one needs a system with infinite bandwidth. However, in that case, the concept of a delta function breaks down when faced with the physical reality that any propagation process is frequency selective, and thus even a single multipath component has its impulse response not as a delta pulse, but rather a *continuous* distortion function whose shape is determined by the particular interaction processes that it undergoes on the way from Tx to Rx [31]. Similarly, in the angular domain, no true "plane wave" is possible, since wavefront curvature due to diffraction and similar effects distort the wavefront. In theory, if all the interaction processes and their distortions are exactly known, it would be possible to modify (1), replacing the delta functions with the appropriate distortion functions in delay and angle, in which case it would still be possible to represent the SCs by a finite sum of fundamental waves. This would leave DS from rough surfaces as the only source of DMC.

1. To be completely general, we would have to include a description of polarization as well. To avoid the cumbersome matrix notation, we omit this case here and refer the interested reader to [29].

We hasten to add that a perfect knowledge of the distortion functions is extremely difficult to achieve and we are not aware of any papers that have attempted modeling in this way. The question also remains where to draw the boundary between small but deterministic objects (e.g., windowsills) and "rough surfaces" - again such a distinction is to a certain degree arbitrary.

For the realistic case of a finite bandwidth, we furthermore note that each resolvable delay bin (or equivalent matched filter output sampled at the Nyquist rate) will contain the integrated, weighted contributions from a continuum of delays, which may consist of both SCs and DMC. This again prevents a perfect separation of DMC and SCs, and it furthermore makes clear that the temporal resolution of the DMC is limited by the bandwidth of the system (similar comments apply to the angular resolution). A large number of small MPCs is not "significantly different" in terms of the low-pass filtered impulse response compared to a DMC, while fewer, stronger, MPCs can be clearly distinguished. However, the reader will recognize that a wording like "significantly different" leaves a certain ambiguity in the distinction criterion.

Another point of view arises from analysis of the measurement results. As will be shown in Section IV, high-resolution parameter estimation (HRPE) describes both the SCs and the DMC by a small set of parameters. For the SCs, these parameters are obviously the a_ℓ, τ_ℓ, Ω_ℓ, and ψ_ℓ. The DMC is described, e.g., as a single-exponential decay in the delay domain and uniformly distributed in angle, so that only two parameters (decay constant and amplitude) are required. The HRPE then matches these model parameters to the observable signals (impulse responses at the different antenna elements). Due to the impact of noise, the parameters cannot be extracted exactly, even if the assumptions of the model are fulfilled exactly. As follows from the Cramer-Rao Lower Bound, weaker components have larger errors associated with them, so that for MPCs below a certain threshold, any estimated parameters become essentially meaningless. It thus follows also from this perspective that a - somewhat arbitrary - threshold must be chosen, such that only SCs stronger than this threshold are estimated (or are meaningful when estimated); weaker contributions are advantageously assigned to the DMC even if their physical origin (e.g., specular reflection) would indicate their nature as SC.

A low-parametric DMC model might provide a significant model mismatch with the reality. For example, a uniform angular distribution of the DMC around a Tx might not be realistic depending on the surroundings of the Tx. Improved representation can then be either achieved by a DMC model with larger number of parameters, or by leaving a low-parametric DMC model and add more small SCs. Again, the choice between the two is somewhat a matter of taste.

To summarize, it does not seem possible to provide a strict distinction between SC and DMC either mathematically (pure delta functions do not exist for real-world electromagnetic waves), physically (where to draw the line between small deterministic objects and random roughness), or from a measurement point of view (finite bandwidth and impact of noise). Rather, a pragmatic separation has to be done that depends on the bandwidth, signal-to-noise ratio (SNR), as well as the degrees of freedom of the DMC model. It is certainly unsatisfactory that the representation has so many degrees of arbitrariness, but as we have expounded above, this is a consequence of very fundamental propagation principles.

The above derivation has been based on the expansion of the electromagnetic field into plane waves. An alternative expansion is based on spherical vector waves (SVWs), which can describe well the fields emitted by small antennas, with the naturally discrete and orthogonal basis of SVW modes truncated by the electrical size of antennas. The transformation of the expansion coefficients when changing between these two descriptions was described in [32]. In particularly, in [33], the authors proposed to use the SVW channel modeling approach to model the nonspecular wave scattering from rough surfaces. In the paper, the performances of the plane wave modeling in [34] and the SVW channel modeling in [35]–[37] on characterizing the nonspecular wave scattering components were compared, where the ground truth was the scattering computed by physical optics (PO). Results showed that the SVW modeling method is more efficient to model the nonspecular components, representative for DMC. However, it is worth noting that SVWs may be well suited to describe DMC, since those generally have a smooth angular variations; however, they are not a natural fit for the SCs.

III. MODELING OF DMC

A. OVERVIEW OF DMC MODELING

As discussed above in Section II, a multipath propagation channel can be represented by the SCs and the DMCs. It is well known that SCs can be modeled deterministically, e.g., through ray tracing, or stochastically. For simplicity, many standardized channel models consider only SCs, such as 3rd Generation Partnership Project (3GPP) spatial channel model (SCM) [38], ITU-R P.1238 channel model [39], ITU-R P.1411 channel model [40], and WINNER II channel model [41], [42]. Further, ITU-R recommendation P.1238 on multipath propagation modeling and parameterization [43] has not yet considered the DMC. This simplification leads to the model mismatch problem in some scenarios where DMC contributes significantly. To fill up the gap, a suitable model for the DMC has to be added to the SC contributions of the impulse response.

There are mainly three ways to model DMC, namely, stochastic and geometry-based stochastic modeling, and deterministic modeling. In the former case, the angular delay power spectrum of the DMC is modeled, and instantaneous realizations of the DMC are created based on the fading statistics in each resolvable delay/angle bin; the fading amplitude statistics are commonly assumed to be zero-mean complex Gaussian. Alternatively, the geometry-based stochastic approach is applied, in which discrete diffuse

scatterers are placed randomly, according to theoretical or empirical statistical distributions. The contributions of the scatterers are determined by using simplified RT. All contributions of the scatterers are summed up in order to obtain the overall DMC. This approach is commonly used in conjunction with geometry-based stochastic modeling of SCs.

For the deterministic modeling of DMC, methods like RT are usually applied and extended by ad hoc models to simulate DMC. In this kind of models, the DMC is considered as a result of interactions between the radio signals and scattering objects with rough surface [44]. It can be treated as noncoherent components that are scattered by scattering objects into nonspecular directions. The improved RT based model includes the DMCs from different objects.

We summarize in Table 1 the modeling methods of DMC in various papers in the literature. In the following, we discuss the modeling approaches of DMC in detail.

B. STOCHASTIC MODELS

Stochastic models, when properly parameterized, provide a valuable phenomenological description of the DMC, though they are not tied directly to the physics.

An observation of the complex channel transfer functions in a MIMO system can be written as the following vector [4]

$$\boldsymbol{h} = \boldsymbol{s}(\boldsymbol{\Theta}_s) + \boldsymbol{d}_{dmc} + \boldsymbol{n}, \tag{3}$$

where $\boldsymbol{h} \in \mathbb{C}^{M_R M_T M \times 1}$, M is the number of frequency samples, M_T and M_R are the numbers of transmit and receive antennas, respectively. $\boldsymbol{s}(\boldsymbol{\Theta}_s)$ is the contribution of SCs, where $\boldsymbol{\Theta}_s$ denotes the channel parameters of the SCs. $\boldsymbol{d}_{dmc}$ is the contribution of the DMCs, $\boldsymbol{n}$ denotes measurement noise, which is always present in radio channel measurements. The measurement noise is assumed to be a white complex circularly symmetric Gaussian distributed random vector $\boldsymbol{n} \sim \mathcal{N}_c(\boldsymbol{0}, \sigma^2 \boldsymbol{I}_n)$, where σ^2 denotes the noise variance, $\boldsymbol{I}_n$ denotes an identity matrix with size $M_R M_T M \times M_R M_T M$. $\boldsymbol{h}$ is usually regarded as a random variable that follows the complex multivariate Gaussian distribution, and defined as

$$\boldsymbol{h} \sim \mathcal{N}_c\Big(\boldsymbol{s}(\boldsymbol{\Theta}_s), \boldsymbol{R}(\boldsymbol{\Theta}_d) + \sigma^2 \boldsymbol{I}_n\Big), \tag{4}$$

The mean $\boldsymbol{s}(\boldsymbol{\Theta}_s)$ of the Guassian distribution is determined by the SC, the stochastic part includes DMC and noise, DMC determines the covariance matrix $\boldsymbol{R}(\boldsymbol{\Theta}_d)$. The full covariance matrix $\boldsymbol{R}(\boldsymbol{\Theta}_d)$ is of size $M_R M_T M \times M_R M_T M$, where $\boldsymbol{\Theta}_d$ denotes the parameters of the DMCs. The contribution of DMC can be seen as a multivariate circular complex Gaussian process with zero-mean and covariance matrix $\boldsymbol{R}(\boldsymbol{\Theta}_d)$)

$$\boldsymbol{d}_{dmc} \sim \mathcal{N}_c(\boldsymbol{0}, \boldsymbol{R}(\boldsymbol{\Theta}_d)). \tag{5}$$

A variety of simplified models have been proposed for this covariance matrix.

1) THE KRONECKER MODEL

A major simplification occurs if we assume that the stochastic process is separable, i.e., the spatial correlation functions do not depend on which delay we consider them at, and the spatial correlation function at the Rx is independent of the transmit direction (and vice versa). In this case, the full covariance matrix can be written as the Kronecker product of the temporal correlation matrix, Tx spatial correlation matrix, and Rx correlation matrix [4]

$$\boldsymbol{R}(\boldsymbol{\Theta}_d) = \boldsymbol{R}_{Rx}(\boldsymbol{\theta}_{R,d}) \otimes \boldsymbol{R}_{Tx}\big(\boldsymbol{\theta}_{T,d}\big) \otimes \boldsymbol{R}_F(\boldsymbol{\theta}_d), \tag{6}$$

where $\otimes$ represents the Kronecker product, $\boldsymbol{\theta}_d$ denotes the DMC propagation parameters in the time-delay domain, $\boldsymbol{\theta}_{R,d}$ denotes the parameters of the DMC in angular-polarization domain at the Rx side, $\boldsymbol{\theta}_{T,d}$ denotes the parameters of the DMC in angular-polarization domain at the Tx side. $\boldsymbol{R}_{Rx}(\boldsymbol{\theta}_{R,d}) \in \mathbb{C}^{M_R \times M_R}$ and $\boldsymbol{R}_{Tx}(\boldsymbol{\theta}_{T,d}) \in \mathbb{C}^{M_T \times M_T}$ describe the spatial correlation matrix of the DMC at the Rx and the Tx, respectively. $\boldsymbol{R}_F(\boldsymbol{\theta}_d)$ describes the frequency correlation function of the DMC.

Under the assumption that the DMCs are uniformly distributed in the angular domains, and the antennas are sufficiently spaced apart (at least half a wavelength), the spatial correlation matrices become identity matrices, and the full covariance matrix $\boldsymbol{R}(\boldsymbol{\Theta}_d)$ can be written as

$$\boldsymbol{R}(\boldsymbol{\Theta}_d) = \boldsymbol{I}_{M_R} \otimes \boldsymbol{I}_{M_T} \otimes \boldsymbol{R}_F(\boldsymbol{\theta}_d), \tag{7}$$

where $\boldsymbol{I}_{M_R}$ and $\boldsymbol{I}_{M_T}$ denote an identity matrix with size $M_R \times M_R$ and $M_T \times M_T$, respectively.

More generally, the covariance matrix of DMC in the angular domain can be defined as follows

$$\boldsymbol{R}_A(\boldsymbol{\theta}_A) = \boldsymbol{R}_{Rx}(\boldsymbol{\theta}_{R,d}) \otimes \boldsymbol{R}_{Tx}\big(\boldsymbol{\theta}_{T,d}\big), \tag{8}$$

where $\boldsymbol{\theta}_A$ is the parameters of the DMC in the angular-polarization domain. Substituting (8) into (6), the full covariance matrix $\boldsymbol{R}(\boldsymbol{\Theta}_d)$ can written as follow

$$\boldsymbol{R}(\boldsymbol{\Theta}_d) = \boldsymbol{R}_A(\boldsymbol{\theta}_A) \otimes \boldsymbol{R}_F(\boldsymbol{\theta}_d). \tag{9}$$

It is important to distinguish the Kronecker assumption of the *total* channel (including the SCs) from the Kronecker assumption for the DMC only. While the former has been shown to be rarely fulfilled, in particular when single-reflection processes dominate, the latter assumption might be fulfilled in a much larger range of circumstances. A more accurate analytical channel model is the Weichselberger model [89], which considers the coupling from Tx eigenmodes to Rx eigenmodels. However, to the best of our knowledge it has not yet been applied in the literature to model DMC.

2) DELAY DOMAIN MODEL

A representation of the DMC power delay profile by a single exponentially decaying profile was suggested in [4]. Based on a huge amount of measurement data, the observed power delay profile (PDP) follows a structure with an exponential

TABLE 1. DMC models.

Reference	Modeling approach	Type
[45]	A VMD in angular domain and a linear (angular independent) model for the polarisation domain	Stochastic model
[4], [11]	A single exponential decay in the time-delay domain	Stochastic model
[14], [20]	An exponential decay in the time-delay domain, VMD in angular domain	Stochastic model
[17], [18]	An exponential decay in the time-delay domain, VMD in angular domain	Stochastic model
[19]	A VMD and an additional uniform distribution in angular domain	Stochastic model
[21], [46]	A unimodal VMD and a multimodal VMD in angular domain, an angle-independent polarization vector	Stochastic model
[47]	VMD in angular domain	Stochastic model
[48]	Clusters based model, VMD in angular domain, an exponential decay in time-delay domain	Stochastic model
[49]	Clusters based model, a Fisher–Bingham spectrum in the azimuth-coelevation domain, an exponential decay in time-delay domain	Stochastic model
[50]	Clusters based model, an exponential decay in time-delay domain	Stochastic model
[22], [28]	Multichannel autoregressive model	Stochastic model
[23]	Autoregressive moving average model	Stochastic model
[51]	Moving average model	Stochastic model
[52]	Multidimensional discrete prolate spheroidal sequences	geometry-based stochastic channel model (GSCM)
[53], [54]	Classical GSCM approach	GSCM
[55]	Clusters based model, VMD in angular domain, an exponential decay in time-delay domain, GSCM	GSCM
[56]	Ray-optical wave propagation modeling	Deterministic model
[57]	Ray-launching based model	Deterministic model
[58], [59]	A RT based model	Deterministic model
[60], [61]	A RT model	Deterministic model
[62]	A RT based model	Deterministic model
[63]	A 3D RT algorithm, B-K model, ER model	Deterministic model
[5], [64]	A 3D RT algorithm and B-K model	Deterministic model
[9]	ER model	Deterministic model
[65]	ER dual lobe model	Deterministic model
[24]	A ray-based model, ER model, geometrical optics (GO) rules, uniform geometrical theory	Deterministic model
[66]	A 3D RT and ER model	Deterministic model
[67]	A RT and ER model	Deterministic model
[68]	A RT, ER model	Deterministic model
[69]	A 3D RT and ER model	Deterministic model
[70]	Directive scattering model, radar cross section model	Deterministic model
[71]	Directive scattering model	Deterministic model
[72]	A RT, the directive model	Deterministic model
[73]	The directive model and double-lobe model, RT tool	Deterministic model
[13], [74]	RT tool, Lambertian model	Deterministic model
[75]	Lambertian model, directive model, Backscattering lobe model, ER model, 3D RT tool	Deterministic model
[76], [77]	Lambertian model, directive model, directive with backscatter model, RT tool	Deterministic model
[78]–[80]	The Lambertian model and the directive model, RT tools	Deterministic model
[81]	A phase evolution modeling approach based on ER model	Deterministic model
[82]	A semi-deterministic graph model base on ER approach	Hybrid deterministic and stochastic models
[83]	Point clouds and physical optics	Hybrid deterministic and stochastic models
[84], [85]	Point clouds and single-lobe directive model	Hybrid deterministic and stochastic models
[86]	The PG model and a single-lobe directive model	Hybrid deterministic and stochastic models
[25], [87], [88]	The PG and RT	Hybrid deterministic and stochastic models

decay in delay domain. The PDP of DMC can be represented as [4]

$$\Psi(\tau) = \begin{cases} 0, & \tau < \tau_d' \\ \frac{\alpha_1}{2}, & \tau = \tau_d' \\ \alpha_1 e^{-B_d(\tau - \tau_d')}, & \tau > \tau_d' \end{cases} \tag{10}$$

where τ represents the delay, B_d the coherence bandwidth, α_1 the maximum power, and τ_d' the base delay of the DMCs.

The Fourier transform of $\Psi(\tau)$ is well known as the power spectrum density. Considering a limited bandwidth B, the sampled version of the power spectrum density is given by

$$\boldsymbol{k}(\boldsymbol{\theta}_d) = \frac{\alpha_1}{M}\left[\frac{1}{\beta_d}, \frac{e^{-j2\pi\tau_d}}{\beta_d + \frac{j2\pi}{M}} \cdots \frac{e^{-j2\pi(M-1)\tau_d}}{\beta_d + \frac{j2\pi(M-1)}{M}}\right]^T, \quad (11)$$

where $\beta_d = B_d/B$ is the coherence bandwidth of the diffuse components normalized to the measurement bandwidth B, $\boldsymbol{\theta}_d = [\alpha_1, \beta_d, \tau_d]^T$ is the parameter vector that is used to describe the distribution of the DMC and parameterize the DMC model. τ_d represents the normalized base delay of the DMC, $\tau_d = \tau_d'/T_p$ with the total length T_p of observed channel impulse response, M is the number of frequency samples, f_0 is the frequency sample interval. More description of the parameters can be found in [4]. This model has been widely used for analyzing the characteristics of DMC, as well as for further extensions of modeling the DMC in realistic environment such as the indoor multi-antenna channel [48], [49].

We know that if the uncorrelated scattering (US) assumption is fulfilled, the frequency correlation function is independent of the absolute frequency and only depends on the difference Δf between the two frequencies of interest. In this case, the frequency covariance matrix takes on a Toeplitz form. Specifically, with the single-exponential PDP,

$$\boldsymbol{R}_F(\boldsymbol{\theta}_d) = \Gamma\left(\boldsymbol{k}(\theta_d), \boldsymbol{k}(\boldsymbol{\theta}_d)^H\right), \quad (12)$$

where Γ represents a Toeplitz-matrix, where the first column is defined by $\boldsymbol{k}(\boldsymbol{\theta}_d)$ and the first row is defined by $\boldsymbol{k}(\boldsymbol{\theta}_d)^H$.

3) ANGULAR AND POLARIZATION DOMAINS MODEL

As MIMO systems have been widely used in wireless systems, the DMC becomes a crucial factor for MIMO channel modeling and system performance evaluation. In earlier works, the DMC was assumed to be uniform in the angular domain. Later measurement based studies, however, reveal that the angular-uniform assumption is unrealistic. Reference [18], [90] proposed to model the DMC by a VMD [91].

For DMC, the power angular profile (PAP) regarding the azimuth angle at both transmitter and receiver can be described by the unimodal VMD. For instance, the PAP at receiver can be written as:

$$f_R(\varphi) = \frac{1}{2\pi I_0(k_\varphi)} e^{(k_\varphi \cos(\varphi - \mu_\varphi))}, \quad (13)$$

where φ is the azimuth angle, μ_φ is the symmetry center or "mean angle" of azimuth angle at Rx, $I_0(\cdot)$ denotes the modified Bessel function of the first kind of order zero. k_φ represents the azimuth angular spread of DMC, which is related to the variance of the VMD. It ranges from 0 to ∞, where 0 is corresponding to the case of omnidirectional scattering and ∞ to the case of extremely concentrated. When $k = 0$, the VMD becomes the uniform distribution.

When only the azimuth angle is considered, the spatial covariance matrix $\boldsymbol{R}_{RX}$ can be computed from the PAP as

$$\boldsymbol{R}_{Rx}(\boldsymbol{\theta}_{R,d}) = \int_{-\pi}^{\pi} \boldsymbol{b}_{Rx}\boldsymbol{b}_{Rx}^H f_R(\varphi) d\varphi, \quad (14)$$

where $\boldsymbol{b}_{Rx}$ is the steering vector corresponding to the receiver antenna array and φ is the azimuth angle. This equation does not consider different polarizations.

Similarly, the covariance matrix at the Tx is defined as

$$\boldsymbol{R}_{Tx}(\boldsymbol{\theta}_{R,d}) = \int_{-\pi}^{\pi} \boldsymbol{b}_{Tx}\boldsymbol{b}_{Tx}^H f_T(\varphi) d\varphi, \quad (15)$$

where $\boldsymbol{b}_{Tx}$ is the steering vector corresponding to the transmitter antenna array, $f_T(\varphi)$ is the statistical angular density spectrum of the impinging waves at the Tx.

In the case that both azimuth and elevation are considered, the multivariate (both azimuth and elevation) density of the VMD at the Rx can be modeled by a two dimensional VMD as follows [19]

$$f_R(\varphi, \nu) = \frac{1}{2\pi I_0(k_\varphi) 2\pi I_0(k_\nu)} \mathrm{e}^{k_\varphi \cos(\varphi - \mu_\varphi)} e^{k_\nu \cos(\nu - \mu_\nu)}, \quad (16)$$

where ν is the elevation angle, μ_ν is the symmetry center of elevation angle at Rx. k_ν is the elevation angle spread of DMC. It is worth noting that both azimuth and elevation angles are assumed to be uncorrelated, which allows for an independent and individual estimation.

The spatial covariance matrices in the two-dimensional case require integration over the full solid angle range [19]

$$\boldsymbol{R}_{Rx}(\boldsymbol{\theta}_{R,d}) = \int_{-\pi}^{\pi}\int_{-\pi}^{\pi} \boldsymbol{b}_{Rx}\boldsymbol{b}_{Rx}^H f_R(\varphi, \nu) d\varphi d\nu. \quad (17)$$

Similarly, we can obtain the covariance matrix at Tx side.

In the polarimetric scenarios, the PAP is often modeled by multiplying the VMD with an angle-independent polarization vector $\boldsymbol{\gamma}_d = [\gamma_{d,\varphi\varphi}, \gamma_{d,\varphi\nu}, \gamma_{d,\nu\varphi}, \gamma_{d,\nu\nu}]$ [45]. $\gamma_{d,\varphi\varphi}, \gamma_{d,\varphi\nu}, \gamma_{d,\nu\varphi}$ and $\gamma_{d,\nu\nu}$ are the four complex polarimetric path weights, where the second subscript indicates the polarization at the Tx side, the third subscript indicates the polarization at the Rx side. The angular and polarization domain covariance matrix $\boldsymbol{R}_A(\boldsymbol{\theta}_A)$ is defined as follows

$$\boldsymbol{R}_A(\boldsymbol{\theta}_A) = \boldsymbol{R}_{\varphi\varphi} + \boldsymbol{R}_{\varphi\nu} + \boldsymbol{R}_{\nu\varphi} + \boldsymbol{R}_{\nu\nu}, \quad (18)$$

where $\boldsymbol{\theta}_A = [\mu_\varphi, \mu_\nu, k_\varphi, k_\nu, \gamma_{d,\varphi\varphi}, \gamma_{d,\varphi\nu}, \gamma_{d,\nu\varphi}, \gamma_{d,\nu\nu}]$ is the parameters of the DMC in the angular-polarization domain. $\boldsymbol{R}_{xy}$ is the covariance matrix in angular domain given a specific polarization set $\{x, y \in \{\varphi, \nu\}\}$, where φ and ν indicate the horizontal and vertical polarization, respectively. $\boldsymbol{R}_{xy}$ is calculated as [45]

$$\boldsymbol{R}_{xy} = \gamma_{d,xy}\boldsymbol{C}_{xy}, \quad (19)$$

where $\boldsymbol{C}_{xy}$ represents the angular power spectrum (APS) considering both transmitter and receiver. It can be calculated by

$$\boldsymbol{C}_{xy} = \boldsymbol{C}_x \otimes \boldsymbol{C}_y, \quad (20)$$

with

$$C_x = \int_{-\pi}^{\pi}\int_{-\pi}^{\pi} \boldsymbol{\alpha}_{T,x}(\varphi, \nu) f_T(\varphi, \nu) \boldsymbol{\alpha}_{T,x}^H(\varphi, \nu) d\varphi d\nu, \quad (21)$$

TABLE 2. Multi-cluster DMC models.

Reference	Approach	The number of clusters
[18]	Each cluster has SCs and DMCs	1
[21]	Multiple clusters exists in the PAP of Tx and Rx	The number of angular DMC clusters varied from 1 to 3
[48]	The total CIR consists of several clusters. Each cluster contains a SC and a DMC	-
[55]	The clusters near BS, near MS, and regular clusters that near both the BS and MS consist of SC and/or DMC; Far clusters consist of SC only	10
[49], [92]	Each cluster has SC and DMCs	The number of clusters mostly ranges from 4 to 6. It can be statistically described by a Poisson distribution plus a constant 3. The Poisson distribution has a mean value of 1.69.
[50]	Each cluster contains one SC and one DMC	7
[93]	One or two strong paths were followed by several DMCs	The number of clusters varied from 6 to 9
[94]	A cluster contains a strong SC accompanied by several diffuse clutter	The number of clusters has a mean value of 5, ranging between 4 and 6.

$$C_y = \int_{-\pi}^{\pi}\int_{-\pi}^{\pi} \boldsymbol{\alpha}_{R,y}(\varphi, \nu) f_R(\varphi, \nu) \boldsymbol{\alpha}_{R,y}^H(\varphi, \nu) d\varphi d\nu, \quad (22)$$

where $\otimes$ represents the Kronecker product. In the above equations, $\boldsymbol{\alpha}_{T,x}$ is the Tx array response for the polarization set x, and $\boldsymbol{\alpha}_{R,y}$ the Rx array response for the polarization set y. $f_T(\varphi, \nu)$, $f_R(\varphi, \nu)$ denotes the APS density of Tx side and Rx side, respectively.

It is worth noting that so far a single cluster was considered. However, the single cluster hypothesis is not always valid in reality. Therefore, further extensions have been made to multiple clusters, where the DMC was modeled by multimodal distribution instead of a unimodal distribution. In the following, we discuss this case in detail.

4) MULTI-CLUSTER MODELS

Measurements have shown that multiple clusters can exist in the PAP of Tx and Rx side of the DMC. In that case, the angular probability density function (PDF) at Rx side is modeled by a mixture of angular PDFs:

$$f_R(\varphi, \nu) = \sum_{c_r=1}^{Q} \varepsilon_{c_r} f_R^{c_r}(\varphi, \nu), \quad (23)$$

where Q denotes the number of clusters, ε_q $(q = 1, 2, \ldots, Q)$ are unknown mixture proportions with the constraint of $\sum_{c_r=1}^{Q} \varepsilon_{c_r} = 1$, $f_R^{c_r}(\varphi, \nu)$ is defined as any valid angular PDF at the Rx side [17]. Similarly, we can obtain the angular PDF at the Tx side. The covariance matrices for the polarized case can be generalized similarly

$$R_{xy} = \sum_{c_t=1}^{c_T}\sum_{c_r=1}^{c_R} \gamma_{d,xy}^{c_t,c_r} C_{xy}^{c_t,c_r}, \quad (24)$$

where c_T, c_R are the number of clusters in the PAP of Tx and Rx, respectively. $\boldsymbol{C}_{xy}^{c_t,c_r}$ is the combined Tx and Rx covariance matrix of the c_t, c_r cluster that can be computed like in the single-cluster case.

In [55], the DMC is modeled as a superposition of 10 DMC clusters and incorporated into the geometry-based stochastic channel model (GSCM) framework, though not every cluster is associated with a DMC in this model. Four major types were considered in the paper: while clusters close to base station (BS), close to mobile station (MS), and regular clusters that are near both the BS and MS consist of SC and/or DMC, far clusters consist of SC only. In [50], the DMC is modeled as a superposition of seven clusters, each consisting of one SC and one DMC. Table 2 summaries the cluster-based DMC modeling methods.

5) AUTOREGRESSIVE MODEL

In [22], [28], the DMC is treated as a stochastic process and modeled by a MAR model. Due to its simplicity in terms of obtaining the parameters using the matrix-valued equations, the autoregressive (AR) model has been widely used for simulating some typical fading channels like the Rayleigh fading channel and frequency selective channel. Using AR to model the DMC has been validated in the literature where the parameters are jointly estimated with the SC. More details on estimation are presented in Section IV.

C. DETERMINISTIC MODELS

In the past decades, deterministic methods to model the DMC have been studied. In particular, RT has been modified by including DS from various objects (i.e., building walls, furniture, vehicles etc.) [24], [58]. Based on the constructed environment, physical approaches are applied to simulate the diffuse component such as the "ER" [24], [68], [75], "Beckmann- Kirchhoff (B-K) model" [5], [63], [64], and the "multiple-facets model" [56]. Reference [24] proposed a 3-D model that is partly based on geometrical optics (GO)/uniform geometrical theory of diffraction (UTD) and partly on ER for evaluating the DS by building walls. A sort of ER is associated with each wall, which considers surface roughness and surface/volume irregularities. In addition, some authors established phase correlation models for DS in the ER approach. Reference [81] considered the spatial-dependent connections of tile field phases (i.e., the phases of

the field on different tiles into which the surface of interest is divided), proposed a phase evolution model for DS in the ER approach, and validated the model by simulations and measurements. It is worth mentioning that the simulation reference used in this paper is the PO [95]–[97], which is a standard high frequency approximation to solve the Maxwell's equations. To apply PO, a rough surface with surface irregularity is divided into meshes that are small enough compared to the wavelength and each mesh is considered as locally planar. PO provides decent accuracy for the lit region of source, is applicable for different shapes with low curvature, and is less computation-complex compared to the rigorous full-wave approaches where the induced currents are determined by a large set of linear equations hence maybe extremely time-consuming. Reference [63] implemented ER and B-K model, and evaluated the diffuse scattering for different situations in terms of roughnesses and dielectric constants of the random surface. Reference [64] presents a 3-D RT algorithm based on the B-K model for modeling DS as the non-specular component at Terahertz (THz) frequency band. In [5], again the B-K model was used for modeling diffuse scattering mechanism in RT, based on which the impact of DS on massive MIMO over NLoS channels at THz frequencies. In [44], [98], authors established a diffuse scattering polarization model that is compatible with ray tracing method. The proposed model was extended considering the field polarization behaviour of DS, and validated in reference scenarios where isolated buildings are present.

In addition, the directive and Lambertian diffuse models, derived from the ER model, have been used in several works to incorporate DMC in RT tools, e.g., [74], [75], [78]. In [74], the Lambertian model was used to implement the diffuse scattering in RT tool. In [75], the ER model, suitable to introduce scattering in ray-based propagation models, is described. Authors use three sub-models (i.e., the Lambertian model, the directive model, and the backscattering-lobe model) based on different scattering patterns. These patterns are related to the direction of incidence of the rays incident on a rough surface, and thus establish a physical connection between an SC ray and the associated diffuse scattering. In [78], two different diffuse models, namely, the Lambertian model and the directive model were integrated with an RT tool considering diffuse scattering. In [73], the directive model and double-lobe model are used, which integrated with an RT tool to simulate the diffuse multipath propagation for rough materials. In [84], [85], the room structure was described by a large point cloud; a single-lobe directive model was proposed to calculate the electromagnetic field scattering from a small surface and describe the overall field as fully diffuse backscattering from the point cloud. The results at 60 GHz were validated by comparison to measurements.

The DMC is caused by rough surfaces or small objects, which is however cannot be described in the database of the RT software. Some authors proposed to implement the diffuse scattering in the RT tool. Wall irregularities like windows, balconies, indentations, irregular brick, surface roughness, etc., significantly influence the shape of the scattering pattern, different kinds of scattering models are suitable for different diffuse scattering conditions.

1) LAMBERTIAN MODEL

The scattering radiation lobe of the Lambartian model has its maximum in the direction perpendicular to the surface. The amplitude of the scattered field from a surface element dS can be written as [13], [74]:

$$|E_S|^2 = E_{S0}^2 \cdot \cos(\theta_S) = \frac{K_0^2 \cdot S^2 \cdot \cos(\theta_i) \cdot \cos(\theta_S)}{\pi L_i^2 L_S^2} \cdot dS, \tag{25}$$

where L_i is the distance between the transmitter and the impact point, L_S is the distance between the receiver and the impact point. S is the scattering coefficient, $S = E_S(U)/E_i(U)$, where E_S is the amplitude of the scattered field, E_i is the amplitude of the incident field, and U is the scattering point. $K_0 = \sqrt{60 G_{Tx} P_{Tx}}$, P_{Tx} is the input power to the Tx antenna, G_{Tx} denotes the gain of the Tx antenna. θ_i and θ_S are the incident and departure angles, respectively.

2) DIRECTIVE MODEL

The directive model is also named as single-lobe model. The scattering lobe is steered towards the direction of specular reflection. This model ignores backscatter. The scattered field can be computed as it follows [75]:

$$|E_S|^2 = E_{S0}^2 \cdot \left(\frac{1 + \cos(\vartheta_o)}{2} \right)^{\rho_o}, \tag{26}$$

where angle ϑ_o is the difference between the reflected wave and the scattering direction, ρ_o is related to the width of the scattering lobe. The greater ρ_o, the narrower the scattering lobe. The maximum amplitude E_{S0} can be computed by [75]:

$$E_{S0}^2 = \left(\frac{SK}{L_i L_S} \right)^2 \frac{dS \cos(\theta_i)}{Z_{\rho_o}}, \tag{27}$$

where Z_{ρ_o} is:

$$Z_{\rho_o} = \frac{1}{2^{\rho_o}} \cdot \sum_{j=0}^{\rho_o} \binom{\rho_o}{j} \cdot O_j, \tag{28}$$

and

$$O_j = \frac{2\pi}{j+1} \cdot \left[\cos(\theta_i) \cdot \sum_{w=0}^{\frac{j-1}{2}} \binom{2w}{w} \cdot \frac{\sin^{2w}\theta_i}{2^{2w}} \right]^{\left(\frac{1-(-1)^j}{2}\right)}. \tag{29}$$

3) BACKSCATTERING LOBE MODEL

The backscattering lobe model is also called double-lobe model. The backscattering lobe model is similar to the directive single-lobe model. However, an extra scattered lobe in the incident direction is considered in the backscattering lobe model (i.e., backscattering phenomena). This model is

suitable for describing diffuse scattering propagation characteristics caused by materials with highly undulating surfaces. The diffuse electric field of double-lobe model can be calculated by [75]:

$$|E_S|^2 = E_{S0}^2 \cdot \left[\Lambda \left(\frac{1+\cos(\vartheta_o)}{2} \right)^{\rho_o} + (1-\Lambda) \left(\frac{1+\cos(\vartheta_i)}{2} \right)^{\rho_i} \right], \tag{30}$$

where ϑ_i represents the angle between the incident direction and scattering direction, ρ_i determine the width of the back-lobe. If ρ_i increases, the width of the lobe decrease. Λ is the so-called repartition factor between the amplitudes of the two lobes. The range of Λ is from 0 to 1. If $\Lambda = 1$, the model can be simplied to the single-lobe model.

For the double-lobe model, E_{S0}, the maximum amplitude of the scattered field, is depending on the incidence, reflection and scattering directions. E_{S0} can be written as [75]:

$$E_{S0}^2 = \left(\frac{SK}{L_i L_S} \right)^2 \frac{dS\cos(\theta_i)}{Z_{\rho_i,\rho_o}}, \tag{31}$$

where

$$Z_{\rho_i,\rho_o} = \frac{\Lambda}{2^{\rho_o}} \cdot \left[\sum_j^{\rho_o} \binom{\rho_o}{j} \cdot O_j \right] + \frac{(1-\Lambda)}{2^{\rho_i}} \cdot \left[\sum_j^{\rho_i} \binom{\rho_i}{j} \cdot O_j \right], \tag{32}$$

and

$$O_j = \frac{2\pi}{j+1} \cdot \left[\cos(\theta_i) \cdot \sum_{w=0}^{\frac{j-1}{2}} \binom{2w}{w} \cdot \frac{\sin^{2w}\theta_i}{2^{2w}} \right]^{\left(\frac{1-(-1)^j}{2}\right)}. \tag{33}$$

In general, RT models enables site-specific and accurate simulations of propagation channel. However, it also suffers from the drawback of high computational complexity. To achieve a balance between complexity and performance, hybrid modeling approaches (see Section III-E) are sometimes adopted.

D. GEOMETRY-BASED STOCHASTIC CHANNEL MODEL

In GSCMs, the conceptually simplest way of implementing diffuse scattering is to place a large number of (typically isotropic) scatterers in the environment, where each scatterer leads to a small amplitude of the associated MPC. The location distribution of those scatterers is chosen based on geometrical considerations, or to conform with measured characteristics of delay, Doppler, or angle distribution. As a typical example, a GSCM for vehicle-to-vehicle (V2V) channels was proposed in [53], using three different types of scatterers: mobile discrete, static discrete, and diffuse. In order to correctly model the Doppler spread, and in agreement with the geometry of the modeled highway, the positions of the scatterers are restricted within two bands on both side of the road; this model was also used in [99] to compare to tapped-delay line approaches.

However, modeling DMC by a great many scatterers can lead to very high computation times. A number of computationally more efficient simulation methods have been proposed. Reference [52] modeled the DS using multi-dimensional discrete prolate spheroidal sequences (DPSS) channel model. In [55], authors proposed cluster-based DMC model considering delay characteristics, angular characteristics, as well as polarization characteristics, and then incorporated the impact of the DMC into the GSCM framework via the covariance matrices of the DMC.

E. HYBRID MODELS

1) HYBRID MODELS BASED ON PROPAGATION GRAPH MODELING THEORY

PG is a promising approach to establish the DMC model, and it can be generated either stochastically or deterministically. In [25], [82], a semi-deterministic PG modeling method based on the ER model is proposed. This combination approach associates the scatterer distribution with realistic environment objects, and calculates the propagation coefficients based on diffuse scattering theories. The proposed model is suitable for the environments with highly diffuse scattering, e.g., propagation at millimetre wave (mmWave) and THz frequency bands. In this framework, the diffuse components are computed using graph theory, while the SCs are computed off-line using RT; overall complexity of the model is rather high. The approach is validated within the environment of an isolated office building environment at 3.8 GHz and an indoor office environment at 60 GHz. A unified PG modeling approach for 60 GHz was proposed in [86], which considered both SCs and DMCs. In the proposed approach, the multiple-bounce diffuse components were modeled by the semi-deterministic PG theory, individual single-bounce SCs and the accompanying diffuse components associated for in-room scenario were simulated by a single-lobe directive model. In [87], a hybrid model was proposed to include deterministic components and the diffuse tail by combining RT with a PG. The deterministic components were provided by RT, the diffuse tail was generated by PG. The parameter settings for the PG are obtained from the environment description via RT and room electromagnetics. Reference [88] combines RT with the PG to predict the intra-room propagation channel. In [87] a different hybrid method is proposed to add the output from RT and PG, where the output information of the scatterers' interactive points from RT was used for the calculation of PG.

2) MIWEBA MODEL

In the Millimeter-Wave Evolution for Backhaul and Access (MiWEBA) channel model [100], [101], the simulated channel impulse response (CIR) is a superposition of so-called D-rays and R-rays. The D-rays contribute the most to the total received power, which is modeled by a geometry-based

deterministic approach. In contrast to the strong D-rays, the R-rays are weaker and reflected by objects in the environment like trees and lamppost, etc. R-rays may have random delays, whose statistical distribution is extracted from channel measurements or detailed RT. Both D- and R-rays can be associated with clusters of weaker components, which can represent DMCs [102]. The model thus has a strong connection to cluster-based DMC modeling.

3) METIS CHANNEL MODEL

The METIS channel model provides different channel model methodologies, such as map-based model, stochastic model and their hybrid model [103]. The METIS map-based model is based on 3D RT principles, in which the propagation environment including random shadowing objects is modeled by a simplified 3D geometrical approach. Propagation mechanisms including direct LoS, specular reflection, diffraction, shadowing due to object blocking, scattering from objects, and diffuse scattering were taken into account [103], [104]. Turning on or off DMC can increase the prediction accuracy or reduce the computational complexity, respectively. The METIS map-based model has also been accepted in the 3GPP model [105] as an alternative model.

IV. CHANNEL PARAMETERS ESTIMATION ALGORITHMS FOR DMC

A number of well-known HRPE algorithms for estimating SCs can be found in literature, which may be based on 1) the subspace approaches such as ESPRIT [106] and the multiple signal classification algorithm (MUSIC) [107], or 2) the iterative maximum likelihood (ML) estimation such as expectation-maximization (EM) [108] and its extension SAGE [109], the gradient-based ML estimator RiMAX [4], and the ML beam-space estimator [110]. In this section, we focus on discussing the algorithms in light of their approach to estimating the parameters of DMC.

A. MAXIMUM LIKELIHOOD ESTIMATION ALGORITHMS

In [4], [26], [111], A. Richter first proposed using the RiMAX multipath estimation method to jointly estimate the parameters of SC and DMC assuming that the DMC is spatially uncorrelated with an exponential decay PDP over time-delay. The proposed ML based approach consists of iterations between estimating the parameters of SC and DMC, with one of them being estimated/updated, while the other one is kept frozen at the previous iteration value. Initialization can be done, e.g., based on a global search (grid search). Within each iteration of the DMC estimation, parameters of the distributed diffuse components are estimated with a ML Gauss-Newton algorithm. The parameters of the SCs are estimated with a Levenberg-Marquardt algorithm using alternating path group parameter updates. The convergence of the parameters is evaluated; once the convergence is reached, the reliability of the propagation paths is checked such that the unreliable paths are discarded. Fig. 3 shows the RiMAX algorithm framework in [4]. In the figure, the red

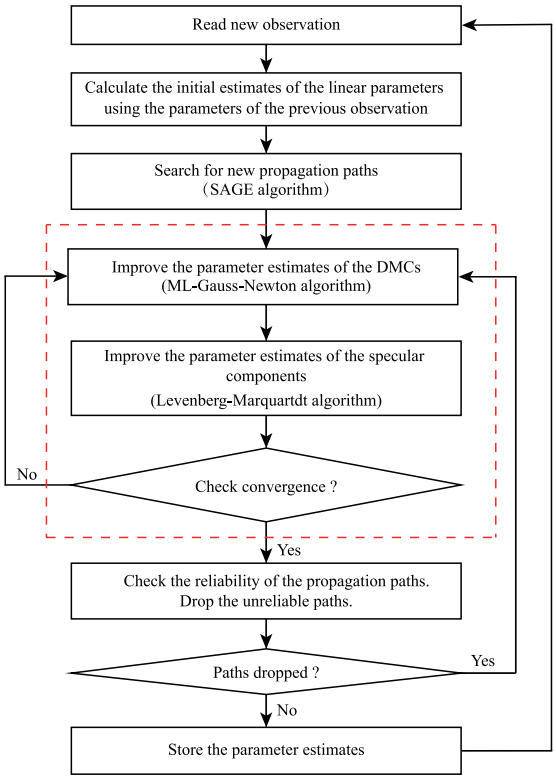

FIGURE 3. The flowchart of the RiMAX algorithm [4].

dotted box is the part of iterative estimation of DMC and SC parameters. More detailed information on RiMAX can be found in [4], and the influences of incomplete and inaccurate data models on RiMAX are discussed in [15]. Based on the RiMAX algorithm framework, several extensions have been made for joint estimation of DMC parameters in frequency, angular, as well as polarization domains [21], [112].

To overcome the drawback of considering only spatially uncorrelated DMC in RiMAX, [45] proposed a more general ML approach for channel estimation considering the spatial correlation of DMC without pre-assumptions on the antenna array structure. In that paper, an iterative ML algorithm is used to obtain the angular DMC parameters from the spatial covariance matrix. The ML approach used the Newton-Raphson algorithm with Fisher-Scoring to solve the ML problem, where the Hessian matrix is replaced by the negative Fisher Information-Matrix. In addition, a Least-Mean-Square (LMS) procedure was used to find initial values for the linear polarisation parameters.

There are few studies on the characteristics of DMC considering both the time-delay domain and the angular domain. The angular-delay domain model results in the correlation matrix with high dimensionality, which increases the complexity of the calculation and makes it difficult to estimate the DMC parameters. In [17], [18], an approximate ML method is proposed to jointly estimate the parameters of the SCs and the DMC. Both spatial and temporal domain

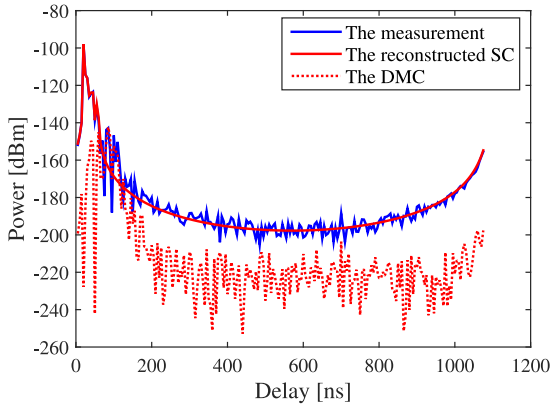

FIGURE 4. An example of the measured power delay profile.

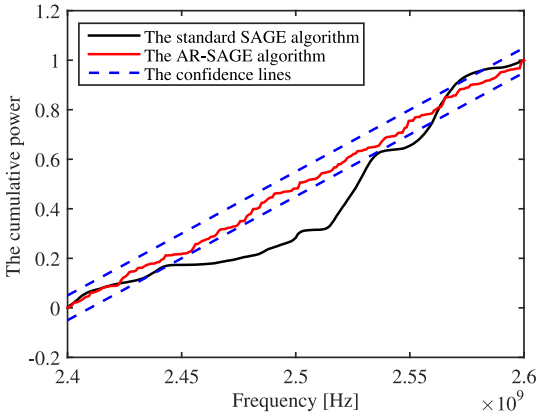

FIGURE 5. The cumulative Periodogram of the residual power spectrum based on the AR-SAGE approach in [22] and the traditional SAGE method.

parameters of the DMC are estimated in an iterative procedure: firstly, the parameters of the SCs are optimized; secondly, the contribution of the SCs is removed from the measurement, and then the covariance matrix of the DMC together with the noise variance are optimized. As for the DMC, the time-delay domain parameters are first estimated. Thereafter, the angular domain parameters are optimized using the estimated time-delay parameters. Such DMC parameter extraction in cluster-based channel models has also been discussed in [49], [50]. For the scattering environment with multiple clusters of scatterers, each cluster is associated with a SC and a diffuse component. In [49], the DMC of clusters is modeled using a Fisher-Bingham spectrum in angular domain, and an exponential PDP including polarization effect, while in [17], [18] the angular power profile is modeled with a mixture of angular VMDs.

Further, [22], [28] propose an ML approach that models the DMC with the AR model. A coupled estimation of parameters of SC and DMC in white noise is achieved. The parameters of SC are estimated by the coupled estimator, where the residual signal after subtracting the estimated SC is used to estimate the AR parameters for DMC. Due to the matrix-valued structure of the parameters of model equations, the autoregressive model parameters can be estimated using Burg's method. Fig. 4 shows an examplary CIR obtained from a measurement campaign with estimated SC and DMC. The cumulative Periodogram of the residual signal is presented in Fig. 5, where the blue dotted line is the 5% confidence line. We can see that the cumulative power of the residual, filtered by the AR-SAGE method, is within the confidence line and the curve fluctuates less.

References [6], [15] show that the estimation performance of the SC can be remarkably enhanced by jointly estimating the SC and the DMC. Particularly, incorporating DMC part into the channel model, as in RiMAX, significantly reduces the influence of model mismatch. Considering only SC may result in an increased number of paths and, thus, an overestimation of the SC. The estimation accuracy of those weak paths will considerably degraded due to low SNR. Furthermore, it is also reported that the estimation performance of the SC may be further enhanced if the information of calibration data model error is known.

B. KF AND EKF PARAMETERS ESTIMATION ALGORITHMS

When time series of channel measurements are available, Kalman filter (KF) and EKF can be used for estimating and tracking the parameters of the MPCs. In [16], the authors focus on estimating and tracking the channel parameters that are represented in the delay domain, where the DMC is modeled by an exponential decay in delay. In this approach, the matrix inversion lemmas are used to reduce the computational complexity and the information form of the EKF is employed to estimate and track the propagation path parameters of DMC. The resulting form of the EKF is robust with low estimation variance and computational complexity compared to the RiMAX estimator. Considering the fact that EKF relies on Taylor series expansion to linearize the non-linear signal model of the propagation channel, the tracking performance of using EKF of path parameters may degrade in scenarios where paths are highly non-linear. Alternatively, a KF based framework, named KEST, to track the path parameters is proposed in [28], [113]. To avoid the linearization problem in highly non-linear scenarios, the static quasi-maximum likelihood based approach SAGE is used as the inner stage to achieve the global maximum in parameter estimation, followed by the outer stage using the KF to track individual estimated paths. The DMC is modeled by the MAR and estimated in the same way as described in last section, where the parameters of SC and the DMC are jointly estimated in a coupled way.

C. BEAMFORMING ALGORITHM

Beamforming is often used to estimate the DMC parameters in the angular domain. In [16], [48], [114], a beamforming technique is used to estimate the PAP of the DMC. In [50], a method is proposed to estimate the SC and the DMC jointly. In the paper, the spatio-temporal spectrum is obtained with double directional Bartlett beamforming, whereas the

parameters of the exponential diffuse PDP is estimated with a least-squares estimator. The Kim-Parks index and the K-power means algorithm are used to extract specular-diffuse clusters from measurement data. In [115], the diffuse models are incorporated into RT tool such that the performance of different beamforming techniques can be assessed, including single-beam and multi-beam effects, in the 60 GHz band.

D. OTHER APPROACHES

Least squares based methods are often used to estimate the PDP parameters of the DMC in the delay domain. In [122], after subtracting the SC that were estimated using the SAGE algorithm, the parameters of the exponential remainder are estimated using a non-linear least squares parameter estimator to determine the PDP of the DMC.

In [123], a sparse Bayesian learning (SBL) algorithm was presented to estimate the dispersion parameters of SC and the power delay profile of the DMC. In contrast to ML and maximum a posteriori estimation where the number of SC is assumed to be known, in the SBL algorithm the number of SCs is unknown and estimated jointly with parameters of SC and DMCs.

In [78], [79], the adjusted parameters approach is used to estimate the best parameters of the directive and Lambertian diffuse scattering models from a block of material. Based on the time and angular response measurement of the material sample, the adjusted parameters method tunes the model parameters. The received power that originates from a zone of the material is evaluated by the time gating method. In the simulation, different sets of parameters are applied under the same scenario. The error function of the Fraction of Variance Unexplained (FVU) has been applied to estimate the difference between the measured and simulated relative received powers. This difference is used to obtained the best model parameters. It is worth noting that the best model parameters may vary depending on environments. The drawback of the algorithm is the high computation time.

As a summary, Table 3 lists the survey of different estimation methods of DMC parameters.

V. MEASUREMENT RESULTS OF DMC

Measurements are the main tool for channel modeling and characteristic analysis. Channel measurements can provide raw data for channel modeling and channel characteristic analysis. Channel measurements include time domain, frequency domain and spatial domain approaches [1]. The time domain approach either measures the channel impulse response in time domain directly by transmitting an impulse signal (impulse sounder) or transmits a signal whose autocorrelation function is an impulse, so that by performing the crosscorrelation between transmitted signal and received signal provides an estimate of the impulse response. The diffuse MPC can usually be seen by inspection in the impulse response if the delay resolution is fine, such that discrete components are resolved and "rise out" of the DMC background. Frequency domain measurements estimate channel the transfer function, where the typical measurement apparatus is a vector network analyzer. DMC is more difficult to identify by inspection in the frequency domain, though of course Fourier transformation to the time domain is possible without loss of information. Further insight into the impulse response structure can be obtained from spatially resolved channel sounding, either by real, synthetic, or switched arrays. Again the DMC can be inspected most easily in the angular domain, since discrete components have an impulse response that is a delta function in angle, and rise out of the diffuse background when viewed in this domain.

While the existence of DMCs, and some fundamental properties, can be assessed from theoretical considerations, ultimately any assessment must be based on, or verified by, measurements. In this section we summarize some of the key results. The description will be mostly qualitative, since the quantitative assessment depends very much on the specific measurement location; readers are referred to the referenced papers for detail. Table 4 and Table 5 summarize measurements of the DMC in terms of energy percentage and delay-angular characteristics, respectively.

Many studies have shown that the DMC parameters are strongly correlated with the discrete channel response. For instance, in the time-delay domain, the base delay of the DMC is correlated with the peak delay of discrete components [122]. It has been also reported that there is a positive correlation between the RMS delay spread of the total impulse response and the ratio of the DMC to total Rx power [122]. In [77], the effects of diffuse scattering in mmWave channels was evaluated. Inclusion of the DMCs increases mean excess delay increased and decreases the root mean square (RMS) delay spread. Overall, is shown that DMC has a significant impact in estimating accurately the channel dispersion, especially in T-shaped or X-shaped street intersections. The peak power of the DMC is likewise correlated with the peak power of discrete components. In [114], it has been shown that in both LoS and NLoS conditions the fraction of DMC over the total power increases when the distance between the transmitter and the receiver increases, and that the power of DMC is concentrated around the same angles and delays as the SC. Moreover, the fading of the DMC is related to frequency: fading occurs at a faster rate at higher frequencies. Some papers found that the DMC power decreases as the frequency increases [125], [129]. However, in [139], DMC has been demonstrated to contribute significantly to the total received power in NLoS condition at mmWave bands, and the contribution of DMC can be higher with increasing frequency. In the cm-wave band (3.1 GHz to 10.6 GHz), [112] observed that the DMC power ratio decreases with increasing frequency. At present, there is no unified conclusion on the relationship between DMC and frequency, therefore, it still needs further study. The DMC to total signal power ratio ranges from 10% to 95% depending on the presence of LoS path, Tx-Rx distance and frequency. Generally the DMC power ratio in NLoS

TABLE 3. DMC parameters estimation methods.

Reference	Estimation approach	Performance analysis	Remarks
[4], [111], [116]	The DMC was considered as a stochastic process, its PDP follows the exponential decay distribution; Jointly estimating SC and DMC, RiMAX, ML-Gauss-Newton and Levenberg-Marquardt algorithm	The PDP of DMC, the power of DMC	Assumed that the DMC is spatially uncorrelated, however, this only holds in specific scenarios
[117]	The conventional RiMAX algorithm	DMC reverberation time, PDP, DMC attenuation loss	The used RiMAX algorithm assumed that the DMC is spatially uncorrelated
[20], [118], [119]	RiMAX algorithm is extended such that the frequency, as well as angular and polarization domain parameters of DMC can be jointly estimated	PDP, power angular delay profile (PADP)	The proposed method has high computational complexity
[21], [46]	Considering multiple angular clusters in the PAP of DMC, extending the estimation of DMC in RiMAX method from unimodal to multimodal in the angular domain; the Levenberg- Marquardt algorithm, the Newton-Raphson algorithm, k-means algorithm, beamforming based method	PAP, angular spread, Mean-Square-Error (MSE) between the residual signal components and its reconstructed spectrum using different DMC angular assumptions, the number of angular DMC clusters	The proposed method has high computational complexity
[45]	A Newton-Raphson based iterative algorithm, LMS method	The MSE of the true DMC parameters compared to estimated DMC parameters	The frequency domain properties of DMC is omitted from the covariance matrix
[17], [18]	An ML based estimator, Levenberg–Marquardt algorithm	PDP, PAP	The results are limited to isotropic linear antenna arrays
[22], [28]	Considering the DMC as a stochastic process with AR filter, jointly estimating SC and DMC, quasi-ML	RMSE of delay, amplitude	Incorporated in SAGE method, increased computational complexity due to additional calculation of AR model coefficients and filtering process
[120]	Exploiting the correlation of the channel parameters in time, EKF is used to estimate SC and DMC	The PDP of DMC	The number of paths is constant. However, due to the path birth and death process in real environment, the instaneous number of paths is no longer constant.
[16], [27], [121]	Considering the DMC as an exponential profile in delay, and an arbitrary angular distribution; the EKF is used to estimate the DMC and SC	PDP, the PADP	An unconstrained estimate of the spatial covariance matrix. The method ignores the actual shape of DMC angular distribution, it cannot be used for antenna independent channel modelling
[114]	EKF, Bartlett beamforming method	DMC to total power ratio, PADP	The used EKF cannot be used for antenna independent channel modelling
[28]	Considering the DMC as a multichannel autoregressive process, KEST	-	The number of SC is assumed to be fixed
[48]–[50]	K-power means algorithm and the Kim-Parks index, beamforming method	PDP, power angular spectra (PAS)	The particular antenna array influences the shape of the beamformer output and distorts the actual PAP of the DMC
[72], [78], [79]	The adjusted parameters approach was used to estimate DS. The measured relative received power and the simulated relative received power are compared to obtain model parameters	PDP, the Fraction of Variance Unexplained	Time-consuming
[122]	Considering the PDP of DMC follows an exponential decay; a non-linear least squares estimator	PDP, the DMC parameters are strongly correlated with the discrete channel response	Assumed DMC with a white azimuthal angular spectrum
[123]	The sparse Bayesian variational method	The PDP of DMC	The number of SCs, SC parameters and DMC parameters are estimated jointly

condition is larger than in LoS condition [8], [112], [127]. Although in some cases, especially LoS scenarios, the contribution of DMC to the total received signal is small, the DMC can still crucially influence the "tail" of the PDP. In [125], [126], [146], the reverberation time of DMC was studied. The reverberation time is metric to describe the decay rate

TABLE 4. Measurements of DMC: percentage of DMC energy.

Reference	Percentage of energy contained in the DMC	Environment	Frequency and bandwidth
[8]	The proportion of DMC in total received power ranges from 10% to 95%; the ratio in NLoS is generally larger than in LoS condition	Indoor office environment with large lobby in the middle	5.3 GHz; 120 MHz
[9]	The DS represents from 5% to 40% of the total power with average value about 20%	An office and a laboratory	3.6 GHz; 200 MHz
[10]	The DMC power ratio increases with frequency but decreases with distance	An underground convoy	32.5 GHz; 15 GHz
[12]	The DMC ratio varies between 23% and 38% in LoS scenarios, varies between 27% and 70% in obstructed line-of-sight (OLoS) scenarios, varies between 57% and 64% in NLoS scenarios	A workshop	3 GHz; 100 MHz
[14]	The DMC ratio is about 15%	An urban macrocell	2.53 GHz; 20 MHz
[20]	The residual power ratios remained more than 30%, the contributions of DMC are not negligible in X-band	Three indoor environments	11 GHz; 400 MHz
[48], [49]	The mean power percentage of the DMC is around 30%	Indoor office environment	3.6 GHz; 200 MHz
[112]	In LoS (NLoS) scenario, the DMC ratio is 50% (60%) for lower UWB frequencies, and 30% (50%) for the higher UWB frequencies	An indoor environment	Frequency ranges from 3.1 to 10.6 GHz, the number of frequency sub-bands is 30, sub-bandwidth is 250 MHz
[114]	In both LoS and NLoS conditions, the DMC power ratio increases when the distance between the transmitter and the receiver increases	Indoor office environment with large lobby in the middle	5.3 GHz; 120 MHz
[124]	The average energy ratios of DMC are 20%, 42%, and 26% for theater, subway station, and lobby, respectively; The maximum power of DMC is distance-dependent and modeled by a linear regression model, Lognormal distributions is used to model the standard deviation (STD) of the maximum power of DMC	Three indoor scenarios	11 GHz; -, 100 MHz, 160 MHz, respectively
[125], [126]	The DMC ratio is a function of the frequency and distance. If the frequency is high, the fading rate of the DMC is also fast. DMC power decreases as the frequency increases. For a given frequency, the reverberation ratio becomes larger as the Tx-Rx separation increases	A laboratory environment	Frequency 2.5 GHz-9.5 GHz, every 500 MHz; bandwidth 100 MHz-900 MHz, every 50 MHz
[127], [128]	The contribution of DMC to the received power varies between 10% and more than 90%	The city center	5.2 GHz; 120 MHz
[129]	The DMC power ratios ranges from 15% to 80%; For the lower UWB frequencies, the DMC ratio is up to 50%; for the higher UWB frequencies, the DMC ratio is down to 30%	An industrial warehouse, a laboratory	The center frequency of 1.35GHz, 80 MHz bandwidth; frequencies range 2-10 GHz, a total of 16 sub-bands, sub-bandwidth is 500 MHz
[130]	There is no strong correlation between the DMC power ratio and the distance between transmitter and receiver, the DMC power ratios ranges from 15% to 80%	An industrial warehouse	1.35 GHz; 80 MHz
[131], [132]	For LoS scenarios, the DMC ratio is 15% ; for OLoS scenarios, the DMC ratio is 40%	A large industrial hall	1.3 GHz; 22 MHz
[133]	The DMC ratio is 10%	A laboratory	Frequency ranges was 57–66 GH; 9 GHz
[134]	The DMC ratio ranges from a few percent to 90%; the DMC ratio is related to the environment	Indoor and outdoor environments	5.2 GHz; bandwidth varies from 20 MHz to 120 MHz
[135]	The PDP of DMC, in the shorter delays the major contribution comes from the SCs; however, at higher delays, the major contribution comes from DMC	-	3.6 GHz; 200 MHz
[136]	The impact of diffused scattering becomes less severe as the distance from the scattering surface and the angle of incidence increases, when directional antennas are employed at both the Tx and Rx	Three different building materials: dressed stone, bath stone, glass	60 GHz; 2 GHz

of the diffuse fields, and it can be calculated from the room electromagnetics theory and electromagnetic fields theory in cavities. For a given frequency, it is found that the reverberation time does not change significantly with the bandwidth up to 900 MHz (or larger) [126]. Furthermore, the reverberation time decreases when the frequency increases [125], [126], [129]. In [131], it is shown that for the Tx–Rx distance less than 15 m, the DMC reverberation time appears to

TABLE 4. ***(Continued.)*** **Measurements of DMC: percentage of DMC energy.**

Reference	Percentage of energy contained in the DMC	Environment	Frequency and bandwidth
[137]	The DMC ratio has a mean value of 6%	Tunnel	5.9 GHz; 30 MHz
[138]	The DMC power decay is quicker as the frequency goes higher	An empty Office, an office in-use, a shopping mall, a railway station platform	Frequency ranges from 61 to 65 GHz, 4 GHz bandwidth; frequency ranges from 69 to 74 GHz, 5 GHz bandwidth
[139]	The contribution of DS in high frequencies is more than that in low frequencies	Urban scenario	2.4 GHz, 28 GHz; -
[140]	DMC ratio is up to 70%, 90% and 65% for the intersection, congestion and OLoS scenarios, respectively	An intersection scenario, congestion scenario, OLoS	5.6 GHz; 240 MHz
[141]	The DMC power is less than 7% in LoS scenario. The DMC is higher in the NLoS scenario, although it is less than 20% in most cases	A conference room	Frequency ranges from 61 GHz to 65 GHz; 4 GHz
[142]	The spatially–unaware version of SAGE found that a DMC hold 14% of the input energy. The spatially-aware version of SAGE found that a DMC hold on average 9% of the input energy	The office buildings	3.6 GHz; 100 MHz
[143]	The power of the DMC is 7-10 dB below the power of the specular paths	The city center	2.53 GHz; 2×40 MHz

be slightly dependent on distance. Moreover, when the Tx-Rx distance is greater than 15 m, the DMC reverberation time has no dependence on distances, and the reverberation times for both LoS and obstructed line-of-sight (OLoS) are close to each other. We note in passing that whenever different frequencies are compared, the different dynamic ranges of measurement equipment at those frequencies need to be taken into consideration.

In terms of the angular characteristics, it has been shown that the APS of the DMC is not uniform in azimuth. Moreover, the angular properties of both SC and DMC are significantly correlated to each other [48]. In [8], it is shown that the energy of DMC is more spread in the angular domain than the SC. In addition, the DMC energy is concentrated around the same angles as for the SC [8], [114].

The dual-polarized MIMO techniques are widely used to improve the radio system performance. Therefore, the DS becomes a crucial key to determine the polarization characteristics of the channel. In [44], the polarimetric properties of DS from building walls are studied. It is shown that the depolarization casued by DS is very low for a simple and homogeneous wall, like a brick wall. For a more complex structure, the depolarization of diffuse rays is significant and can not be discarded. In [145], the polarization behaviour of both SC and DMC in urban environments was analyzed. It was demonstrated that the symmetry of the polarisation matrix is significantly dependent on propagation environment, e.g., LoS, OLoS, and NLoS. The polarization vectors for both SC and DMC are determined according to the angle between the geometric LoS and the street. It was found that the variation of polarization parameters of the SC is much more than the DMC. In this macro cell environment, the objects, like metallic objects, house facades, and clusters far separated etc., can significantly change the polarization behaviour. In [131], [132], the polarization characteristics

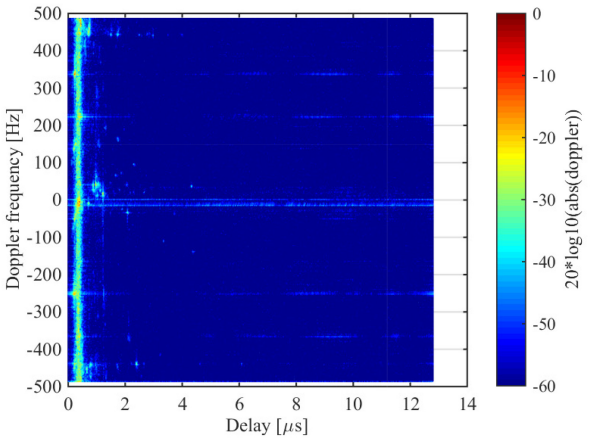

FIGURE 6. **The delay-Doppler spectrum of estimated DMC based on measurement data in a tunnel.**

of both SC and DMC were studied in a large industrial hall environment. The DMC depolarization was found to be weaker in industrial environment than in nonindustrial environments. It can be explained by the fact of the high ceiling. Further, the DMC depolarization is found to be almost constant for all different shadowing, polarizations, and distances. Reference [129] reports that the cross-polar discrimination (XPD) values is not influenced by the distance between transmitter and receiver.

The characteristics of DMCs in Doppler is particularly important in vehicular channels. In [53], [54], results were shown that the DMC has a large delay spread and a large Doppler spread in the highway environment. In the scenario considered in [147], there are two vehicles traveling towards each other along different lanes of the highway. It is shown that the power delay spectrum of the simulated DMC exhibits exponential decay. When the transmitter and

TABLE 5. Measurements of DMC: delay and angular characteristics.

Reference	Decay time constant	Angular spread and polarization behavior	Environment	Frequency and bandwidth
[14]	The maximum power α_1 follows the Gaussian distribution	The concentration parameter k_φ follows the Gaussian distribution	An urban macrocell	2.53 GHz; 20 MHz
[20]	The medians of DMC peak power α_1 ranged between -12 and -9 dB, the CDF of α_1 follows the normal distributions	The medians DMC angular spreads ranged between 80° and 90°; The CDF of k_φ follows the normal distributions; The mean DMC cross-polarization ratio (XPR) ranged between 5.2 dB and 7.7 dB, which were 4 or 5 dB lower than the SC XPRs	Three indoor environments	11 GHz; 400 MHz
[48], [49]	The diffuse cluster base delay ${\tau'}_d$ was correlated with the cluster delay. The concentration parameter k_φ and k_ν are correlated with the inverse of the square sum of the azimuth and coelevation spread. The maximum power α_1 follows the Gaussian distribution	The PAP of DMC is not angular-white, the angular distribution is significantly correlated with the angular cluster location; The diffuse cluster polarization parameters do not show any link to the specular cluster polarization parameters; The peak cross-polar discrimination (XPD) and slope XPD follow Gaussian distribution	Indoor environment	3.6 GHz; 200 MHz
[114]	The decaying of the DMC power is slower than the SC; The delays corresponding to the peaks of the DMC and the SC are the same	The energy concentrations in terms of delay and angular domain are very similar for both DMC and SC	Indoor office environment with large lobby in the middle	5.3 GHz; 120 MHz
[124]	The base delay of DMC is usually within the delay bin of the LOS component	The normalized coherence bandwidth of DMC and its STD are modeled with Lognormal distributions	Three indoor scenarios	11 GHz; -, 100 MHz, 160 MHz, respectively
[125], [126]	For a bandwidth up to 900 MHz or larger, the reverberation time does not change; when the frequency increases the reverberation time decreases	-	A laboratory environment	Frequencies 2.5 GHz-9.5 GHz, every 500 MHz; bandwidth 100 MHz-900 MHz, every 50 MHz
[129]	The reverberation time decreases smoothly when the frequency increases	No significant impact of Tx-Rx distance on the XPD	A laboratory	A center frequency of 1.35GHz, 80 MHz bandwidth; frequencies range 2 GHz-10 GHz, a total of 16 sub-bands, sub-bandwidth is 500 MHz
Reference	**Decay time constant**	**Angular spread and polarization behavior**	**Environment**	**Frequency and bandwidth**
[131], [132]	The reverberation time shows no significant dependence on polarization and distance, i.e., almost constant. If the distance between Tx and Rx is smaller than 15 m, the reverberation time is slightly depending on the distance. If the distance is larger than 15 m, there is no obvious dependence	The copolar (cross-polar) DMC power to total channel power ratio is equal to 15% (40%) for LoS and 40% (60%) for OLoS, there is no correlation between this ratio and Tx-Rx distance	A large industrial hall	1.3 GHz; 22 MHz
[144]	The reverberation time decreases as Tx–Rx distances is increased within 5.5 m; the root mean square (RMS) delay spread of the DMC is higher than for the measured or the SC	-	A laboratory	94 GHz; 3GHz

the receiver have the same velocity, there exists no paths with negative Doppler frequencies of the DMC. When the transmitter and the receiver travel with different velocities, the negative Doppler frequency components appear. Fig. 6 visualizes the delay-Doppler spectrum of estimated DMC based on measurement data in a tunnel scenario. It can be seen that Doppler shifts of the DMCs span a large range.

TABLE 5. ***(Continued.)*** **Measurements of DMC: delay and angular characteristics.**

[8]	-	The DMC energy is more spread in the angular domain than SC, the energy of DMC is concentrated around the same angles as the SC	Indoor office environment with large lobby in the middle	5.3 GHz; 120 MHz
[9]	-	In indoor scenarios, the incoming waves are fully depolarized due to diffuse scattering, as XPD levels are close to 0 dB; The cross-polar components are dominated by DMC	An office and a laboratory	3.6 GHz; 200 MHz
[127], [128]	-	The distributed scattering has usually a wide angular spread at the Tx and Rx	The city center	5.2 GHz; 120 MHz
[44]	-	For a simple and homogeneous wall, DS yields very low depolarization; for a more complex wall structure, the depolarization of diffuse rays is not negligible	Rural building and office building Scenarios	3.8 GHz; 200 MHz
[145]	-	Polarization matrix of DMC is found to be symmetric under NLoS and OLoS environments	A macrocell scenario	4.5 GHz; 120 MHz

VI. IMPACTS OF DMC ON COMMUNICATION, LOCALIZATION AND SENSING

DMC is an important part of radio channel models, which in turn are used for wireless system simulations. If DMC is ignored, it will introduce inaccuracies in simulations for communication, localization, and sensing performance analysis. In the following, we will discuss the impacts of DMC on communication, localization and sensing, separately.

A. COMMUNICATIONS

The DMC could have a significant influence on the performance of communication systems, such as the channel capacity and the information detection accuracy [5], [127]. In particular when the DMC has a large angular spread, it can increase the effective rank, and thus the capacity, of a MIMO system. It has been shown that the impact of DMC on channel capacity strongly depends on individual cases, where in some terrestrial environment the DMC contributes significantly. Depending on the scenario, the DMC may be more dominant in the propagation channel and, therefore, affect channel capacity more than the concentrated propagation paths. In case of LoS scenarios where a strong direct path is present, the influence of DMC on capacity is usually small, though the DMC can lead to an increase of the effective rank at high SNR, in which a larger impact on capacity is possible. In contrast, in case of NLoS scenarios the DMC contributes more power, leading generally to higher spatial multiplexing gain. Conversely, it is reported in [148] that noncoherent non-polarized DMC may reduce the capacity gain of dual-polarized MIMO compared to single-polarized MIMO. Diffuse scattering may be an especially important propagation phenomenon at THz frequencies, and consequently has impact on the channel capacities of THz communication systems. In [5] the capacity of indoor massive MIMO channel at the THz band is studied under both LoS and NLoS conditions with different roughness of surfaces; it was shown that the DS has negative impact on the channel capacity in the LoS scenarios, but DS has positive effect on the channel capacity in the NLoS scenarios. It may enhance the channel capacity under NLoS conditions. DS can also have a significant impact in multi-user MIMO scenarios, in particular when beamforming based on second-order statistics of the channel is used. Due to the larger angular spread, more interference power can "leak" into the receiving beam of a victim receiver.

DMC could result in the deterioration of the channel estimation quality and the consumption of more pilot resources in massive MIMO (mMIMO) communication systems. One distinct feature of mMIMO channel is the sparsity in the frequency, time, or angular domain [149]–[151]. The sparsity has been exploited for reducing the pilot overhead and improving the channel estimation accuracy, such as in the compressive sensing (CS)-based algorithm [152], Bayesian compressed sensing (BCS) [153], [154], orthogonal matching pursuit (OMP) algorithm, subspace pursuit algorithm [155], convex program algorithm, etc. In scenarios that the presence of DMCs is significant but random, it is difficult to obtain the accurate sparsity information of the channel, leading to mismatch between the true channel sparsity and the sparsity estimated by the channel estimation algorithm. A method for joint estimation of sparse SC and DMC in UWB channels was developed in [156], [157].

DMC also influences the channel interpolation and extrapolation that are crucial for certain communication systems. On the one hand, channel interpolation in time or frequency domain is an important aspect of the pilot symbol aided channel estimators in Orthogonal Frequency Division Multiplexing (OFDM) communication systems [158]. Various interpolation techniques have been adopted to improve the estimation accuracy of channel state information (CSI) and reduce the bit error rate (BER), such as linear interpolation, cubic interpolation, spline

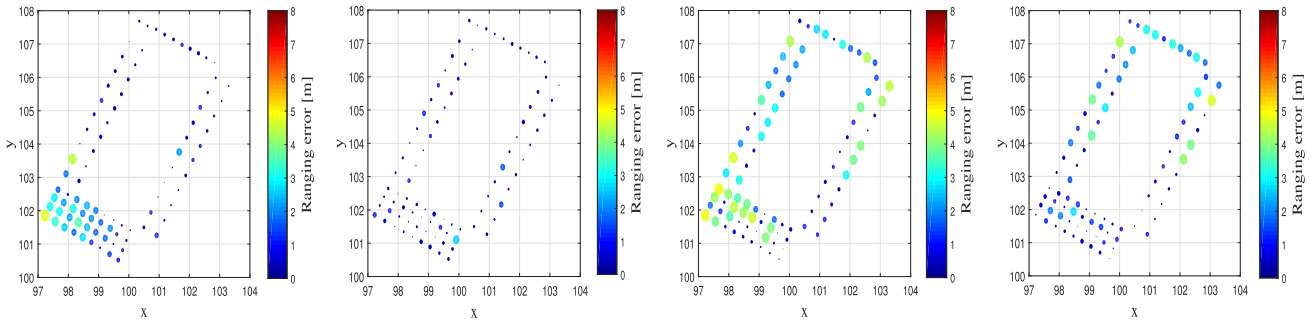

(a) Traditional SAGE algorithm in LOS scenario (b) AR-SAGE algorithm in LOS scenario (c) Traditional SAGE algorithm in NLOS scenario (d) AR-SAGE algorithm in NLOS scenario

FIGURE 7. Comparison of the absolute ranging error achieved by different algorithms in LoS and NLoS environments.

interpolation, polynomial interpolation, adaptive polar linear interpolation, its enhanced version, two-dimensional (2D) adaptive filtering, matrix factorization, and others [159]–[163]. In [7], the authors demonstrated that the misleading frequency interpolation caused by noise (or mal-estimation of DMC) leads to performance degradation. Moreover, the DMC tail of CIR may cause inter-symbol interference, if the cyclic prefix is designed primarily to include the support of the SCs; this breaks the orthogonality of conventional pilot sequences resulting in interference among sub-carriers.

On the other hand, for channel extrapolation it is desired to make use of the available channel information obtained at certain locations and/or frequencies to predict the channels at other locations/frequencies that are not measured/simulated. Such channel extrapolation helps to reduce the requirements for channel state information feedback in frequency domain duplexing systems, and enables better scheduling, since scheduling decisions need to be taken in advance, among other advantages [164]–[166]. Based on channel modeling and parameter estimation algorithms, MPC information like amplitude, phase and angle of arrival is estimated at available locations/frequencies. Based on this information it is possible to form an extrapolated estimate of what the channel will look like at a different location/frequency [166]. It is worth noting that, along with the channel estimation, interpolation, and extrapolation in time-spatial and frequency domains, the array responses or antenna radiation patterns need to be interpolated/extrapolated [167], [168] as well. Using spatial interpolation, coherent interference can be removed, channel capacity can be increased, and interference can be suppressed, see, e.g., [169]. Extrapolation based on HRPE, as well as employing machine learning, has been explored. However, it is worth mentioning that errors originated from measurement, extrapolation algorithm and model mismatch significantly influence the performance of extrapolation [170]. In particular, it is difficult to extrapolate the complex channel state of the DMC, because it behaves stochastically, which then leads to the fact that DMC causes performance degradation of channel extrapolation algorithms.

B. LOCALIZATION AND SENSING

Localization and sensing are envisioned to converge with communications in B5G/6G systems [171], [172], where mono-static or multi-static MIMO or beamforming is utilized for localizing users or sensing (blocking) targets.

It has been found that characterizing DMC improves the localization (or in other words, positioning) accuracy. In [173], the authors propose to locate the user and map the environment by exploiting the DMC rather than considering it as a disturbance. In the paper, the machine learning was used in the context of the localization in a channel with DMC, not for the extraction of the DMC. The tensor-based algorithm was used to estimating the channel parameters of the individual paths within each NLoS cluster. The k-means method was applied in the clustering problem. It is shown that the more diffuse scattering paths used, the smaller the localization error that can be achieved. In [174] a 5G localization and mapping algorithm is proposed, which uses estimated parameters of both SC and DMC to accurately localize, calibrate and synchronize the user equipment. Applying DMC for localization implies that one can still localize the user in the absence of LoS and SCs. In [175], [176], authors proposed a novel likelihood function in the 5G simultaneous localization and mapping (SLAM) filter, which accounts for both the SC and the DMC. The proposed scheme is able to localize and synchronize the user with the assistance of DMC. Fig. 7 shows the ranging performances of both the traditional SAGE and the AR-SAGE algorithm that considers DMC in an office environment. In the figure, individual round dots represent the absolute ranging error at different positions. The radius of the round dot is proportional to the absolute ranging error. Simulation results show that the ranging performance of the AR-SAGE algorithm performs better than the traditional SAGE algorithm in LoS and NLoS scenarios. For the range-based positioning system,

TABLE 6. The impacts of DMC on communication, localization and sensing.

Field	Impact
Communication	DMC affects channel capacity, information detection accuracy, and the performance of channel interpolation and extrapolation algorithms
Localization and sensing	DMC affects localization, tracking and environment mapping accuracy; DMC affects the target detection and separation accuracy.

the better the ranging performance, the higher the positioning accuracy. So, characterizing DMC is helpful to improve localization accuracy. Therefore, through incorporating DMC into channel parameters estimation algorithm and location algorithm, the localization accuracy can be improved.

In terms of contact-free target sensing and DMC, a representative example is human sensing [177], [178]. The backscattered signals from a human body, which can be considered as a rough surface at mmWave or higher frequencies, are mostly diffuse scattering. The scattered fields from human bodies are analyzed in [179]–[181]. The multipath scattering of electromagnetic wave may pose additional problems for signal processing, human detection and tracking. In [182], the ultra-wideband electromagnetic wave scattering from moving humans is considered based on which a human detection and tracking solution was developed. In addition, the multipath scattering affects the performances of target detection and tracking [183]. Since multipath returns can increase or decrease the intensity of the total target signal received by radar, it has advantages and disadvantages for radar detection. The investigations of multipath effect on radar detection mainly focus on using multipath and suppressing it. In [184]–[189], authors improved target detection performance by exploiting multipath reflections. Experimental results verify that multipath improves the radar detection performance for the target. However, it should be noted that the improvement in detection performance is limited.

As a summary, Table 6 lists the survey on the impacts of DMC on communication, localization and sensing systems.

VII. OPEN RESEARCH ISSUES

The previous sections have shown that there is a lot of existing research on the topic of DMC. However, there are still many topics that need to be explored further. These include the establishment of more efficient channel models (combining multiple modeling methods), covering extremely wide frequency bands (such as, THz spectrum, visible light spectrum, etc.), considering more new environments (such as tunnel, underground mine and parking garage, underwater, and human body, etc.), exploring more accurate parameter estimation method (reducing the computational complexity and improving estimate accuracy), and combining with other methods (such as deep learning, machine learning and big data). In particular for new environments and new frequency ranges, more measurements and their evaluation by reliable estimation algorithms are needed as well.

A. CHANNEL MODELS FOR DMC

In countries where 5G communication system have been already deployed, the establishment of accurate DMC models is conducive to a wider application and better performance of these systems. B5G/6G mobile communication systems will incorporate aerial platform like unmanned aerial vehicle, airplane and satellite network in space to realize seamless connection and coverage of sea, ground, and air globally, forming a large-dimensional space-air-ground-underwater network [190], [191]. In this large-scale 3D scenario, the occurrence of DMC is highly likely in both terrestrial and aerial wireless applications. To have a more comprehensive understanding of 6G channel characteristics, accurate channel models including how to accurately incorporate the DMC are necessary for system design and algorithm development. While a variety of model types have been developed, as outlined in Section III, research needs to be done as to whether more efficient and/or accurate models are needed for such convergent 3D models, possibly combining multiple modeling approaches. Further, the reconfigurable intelligent surface (RIS) has also been considered in 6G communication systems, where RIS is envisioned to be useful, to shape and control the smart environment for more reliable and efficient communication. Accurate knowledge of DMC could assist RIS to better control the environment as desired.

B. FREQUENCY-DEPENDENT CHARACTERISTICS OF DMC

Most of the existing work on DMC has concentrated on the traditional cellular bands (1-6 GHz) and - to a lesser extent - the mmWave spectrum. However, the analysis of DMC should cover a wider frequency range, such as the (sub-)THz spectrum or visible light spectrum. Furthermore, the analysis of the frequency-dependence of the DMC characteristics needs to be further improved as well [83], [192], [193]. This is of interest both in order to chose the best operating bands, and because future systems might show frequency dependence between different sub-bands of a system frequency allocation, or even within a subband. In order to fairly compare the frequency-dependent characteristics of the DMC, the same bandwidth, same SNR and same dynamic range should be used during the measurement campaigns.

C. MEASUREMENT ENVIRONMENT

In this paper, the channel measurement environment involved in the existing DMC study are summarized in Table 7. At present, the studies on the characteristics of DMC mainly focus on indoor environments. However, some critical scenarios like tunnels, parking garages, street crosses,

TABLE 7. Channel measurement environment.

Environment		Reference
Indoor	Office	[8], [9], [25], [44], [48], [49], [65], [117], [122], [138], [141]
	Laboratory	[9], [72], [112], [123], [125], [126], [129], [144]
	Hall	[20], [21], [46], [55], [118], [119], [131], [132]
	Shopping mall	[138]
	Station	[124], [134], [138]
	Warehouse	[80], [130]
	Theater	[124]
	A room	[20], [87]
	Underground convoy	[10]
	Museum	[20]
	Lobby	[124], [134]
	Outdoor to indoor	[22], [28]
	Room to room	[88], [121], [195]
	Indoor wall	[66], [78]
Outdoor	Urban	[14], [24], [58], [59], [62], [76], [77], [120], [134], [139]
	City center	[16], [47], [127], [128], [143]
	Rural	[44], [53], [54]
	Street	[11], [57], [111], [134]
	Intersection	[13], [74], [140]
	Highway	[52], [53]
	Tunnel	[137]
	Bridge	[134]
	Tower	[134]
	Square	[134]
	Outdoor wall	[60], [78], [82], [83]

roundabouts, overpass, human body, clothing and vegetation regions can exhibit dominant DMC and have been rarely investigated. In addition, air-to-ground channels and air-to-air channels, which are relevant for 5G and 6G systems, may contain diffuse components [194], however, the characteristics and models of diffuse scattering components of these channels are currently missing in the literature, and suitable measurement campaigns are needed. Marine communication is another environment involving DMC due to rich scattered multipath components on rough sea surface. Channel measurement and analysis with respect to DMC in maritime scenario is also necessary. Moreover, there are a large number of DMCs in V2V propagation environments, and the channel characteristics of vehicular networks can be understood more comprehensively by accurately modeling the DMCs of vehicular networks. However, related works on DMC study in Vehicular ad-hoc network (VANET) environments are quite rare. More channel measurements, establishing the general DMC model and standardizing the DMC model under different scenarios are particularly necessary.

D. PARAMETERS ESTIMATION

Currently, most estimation methods of DMC parameters are based on the RiMAX framework. These methods can be slow in convergence when paths are correlated or not sufficiently decoupled. It is necessary to reduce the computational complexity while keeping parameter estimate accuracy, particularly for those real time positioning application using estimated parameters of DMC to enhance the positioning performance.

VIII. CONCLUSION

In this paper, we presented a comprehensive review of the key topics for DMC in terms of modeling, parameter estimation, characterization, and impact on wireless applications. Different approaches for representing and modelling the DMC in delay domain and angular domain have been categorized. There are mainly three types of representation of DMC, i.e., deterministic models, GSCMs and stochastic models. After discussion of the individual representations and models of DMC, corresponding parameter estimation methods are summarized in terms of snapshot based ML estimators and Bayesian estimators like KF based approach and the EKF approach. Measurement results of the DMC like energy percentage, distance dependency, angular and polarization properties, and Delay-Doppler behavior have also been summarized, and the impact of the DMC on communications, localization and sensing was reviewed. Finally, future open research topics were outlined. Modeling the DMC should be considered within wider frequency spectrum and large scale 3D scenarios for future applications. To this end, models in different frequency bands in diverse environments need to be developed for future wireless applications.

REFERENCES

[1] A. F. Molisch, *Wireless Communications*. Chichester, U.K.: Wiley, 2010.

[2] T. S. Rappaport, *Wireless Communications: Principles and Practice*. Upper Saddle River, NJ, USA: Pearson Ed. Inc., 2002.

[3] K. Haneda *et al.*, "Chapter 2—Radio propagation modeling methods and tools," in *Inclusive Radio Communications for 5G and Beyond*, C. Oestges and F. Quitin, Eds. Amsterdam, The Netherlands: Academic, 2021, pp. 7–48. [Online]. Available: https://www.sciencedirect.com/science/article/pii/B9780128205815000080

[4] A. Richter, "Estimation of radio channel parameters: Models and algorithms," Ph.D. dissertation, Dept. Elektrotechnik und Informationstechnik, Technische Universittät Ilmenau, Ilmenau, Germany, 2005.

[5] F. Sheikh, Y. Gao, and T. Kaiser, "A study of diffuse scattering in massive MIMO channels at terahertz frequencies," *IEEE Trans. Antennas Propag.*, vol. 68, no. 2, pp. 997–1008, Feb. 2020.

[6] D. P. Gaillot *et al.*, "Accuracy of specular path estimates with ESPRIT and RiMAX in the presence of measurement-based diffuse multipath components," in *Proc. 5th Eur. Conf. Antennas Propag. (EUCAP)*, 2011, pp. 3619–3622.

[7] P. Nian and R. Liu, "Anticipated rife interpolation algorithm for frequency estimation of sinusoid signal," in *Proc. IEEE Int. Conf. Power Intell. Comput. Syst. (ICPICS)*, 2019, pp. 287–291.

[8] J. Poutanen, J. Salmi, K. Haneda, V.-M. Kolmonen, and P. Vainikainen, "Angular and shadowing characteristics of dense multipath components in indoor radio channels," *IEEE Trans. Antennas Propag.*, vol. 59, no. 1, pp. 245–253, Jan. 2011.

[9] F. Mani, E. M. Vitucci, F. Quitin, V. Degli-Esposti, and C. Oestges, "Parameterization of a polarimetric diffuse scattering model in indoor environments," *IEEE Trans. Antennas Propag.*, vol. 62, no. 8, pp. 4361–4364, Aug. 2014.

[10] F. Challita *et al.*, "On the contribution of dense multipath components in an intrawagon environment for 5G mmW massive MIMO channels," *IEEE Antennas Wireless Propag. Lett.*, vol. 18, pp. 2483–2487, 2019.

[11] A. Richter, T. U. Ilmenau, A. Richter, and R. S. Thomä, "Parametric modelling and estimation of distributed diffuse scattering components of radio channels," COST 273, Prague, Czech Republic, Rep. TD(03)198, Sep. 2003, pp. 1–15.

[12] E. Tanghe, D. P. Gaillot, M. Liénard, L. Martens, and W. Joseph, "Experimental analysis of dense multipath components in an industrial environment," *IEEE Trans. Antennas Propag.*, vol. 62, no. 7, pp. 3797–3805, Jul. 2014.

[13] V. Degli-Esposti and H. L. Bertoni, "Evaluation of the role of diffuse scattering in urban microcellular propagation," in *Proc. Gateway 21st Century Commun. Village (VTC-Fall) IEEE VTS 50th Veh. Technol. Conf.*, vol. 3, 1999, pp. 1392–1396.

[14] S. Sangodoyin *et al.*, "Cluster characterization of 3-D MIMO propagation channel in an urban macrocellular environment," *IEEE Trans. Wireless Commun.*, vol. 17, no. 8, pp. 5076–5091, Aug. 2018.

[15] M. Landmann, M. Kaske, and R. S. Thoma, "Impact of incomplete and inaccurate data models on high resolution parameter estimation in multidimensional channel sounding," *IEEE Trans. Antennas Propag.*, vol. 60, no. 2, pp. 557–573, Feb. 2012.

[16] J. Salmi, A. Richter, and V. Koivunen, "Detection and tracking of MIMO propagation path parameters using state-space approach," *IEEE Trans. Signal Process.*, vol. 57, no. 4, pp. 1538–1550, Apr. 2009.

[17] C. Ribeiro, A. Richter, and V. Koivunen, "Stochastic maximum likelihood estimation of angle- and delay-domain propagation parameters," in *Proc. IEEE 16th Int. Symp. Pers. Indoor Mobile Radio Commun.*, vol. 1, 2005, pp. 624–628.

[18] C. B. Ribeiro, A. Richter, and V. Koivunen, "Joint angular- and delay-domain MIMO propagation parameter estimation using approximate ML method," *IEEE Trans. Signal Process.*, vol. 55, no. 10, pp. 4775–4790, Oct. 2007.

[19] M. Kaske, M. Landmann, and R. Thoma, "Modelling and synthesis of dense multipath propagation components in the angular domain," in *Proc. 3rd Eur. Conf. Antennas Propag.*, 2009, pp. 2641–2645.

[20] K. Saito, J.-I. Takada, and M. Kim, "Dense multipath component characteristics in 11-GHz-Band indoor environments," *IEEE Trans. Antennas Propag.*, vol. 65, no. 9, pp. 4780–4789, Sep. 2017.

[21] B. Hanssens, K. Saito, E. Tanghe, L. Martens, W. Joseph, and J.-I. Takada, "Modeling the power angular profile of dense multipath components using multiple clusters," *IEEE Access*, vol. 6, pp. 56084–56098, 2018.

[22] T. Jost, W. Wang, D. Shutin, and F. Antreich, "Using an autoregressive model for DMC," in *Proc. 6th Eur. Conf. Antennas Propag. (EUCAP)*, 2012, pp. 3504–3508.

[23] S. Jiang, W. Wang, T. Jost, P. Peng, and Y. Sun, "An ARMA-filter based SAGE algorithm for ranging in diffuse scattering environment," *IEEE Trans. Veh. Technol.*, vol. 71, no. 3, pp. 3361–3366, Mar. 2022.

[24] V. Degli-Esposti, D. Guiducci, A. de'Marsi, P. Azzi, and F. Fuschini, "An advanced field prediction model including diffuse scattering," *IEEE Trans. Antennas Propag.*, vol. 52, no. 7, pp. 1717–1728, Jul. 2004.

[25] L. Tian, V. Degli-Esposti, E. M. Vitucci, and X. Yin, "Semi-deterministic radio channel modeling based on graph theory and ray-tracing," *IEEE Trans. Antennas Propag.*, vol. 64, no. 6, pp. 2475–2486, Jun. 2016.

[26] R. S. Thoma, M. Landmann, and A. Richter, "RIMAX—A maximum likelihood framework for parameter estimation in multidimensional channel sounding," in *Proc. Int. Symp. Antenna Propag.*, Sendai, Japan, Jan. 2004, pp. 1–4.

[27] A. Richter, J. Salmi, and V. Koivunen, "An algorithm for estimation and tracking of distributed diffuse scattering in mobile radio channels," in *Proc. IEEE 7th Workshop Signal Process. Adv. Wireless Commun.*, 2006, pp. 1–5.

[28] T. Jost, W. Wang, U.-C. Fiebig, and F. Perez-Fontan, "Detection and tracking of mobile propagation channel paths," *IEEE Trans. Antennas Propag.*, vol. 60, no. 10, pp. 4875–4883, Oct. 2012.

[29] A. Molisch and F. Tufvesson, "Multipath propagation models for broadband wireless systems," in *Digital Signal Processing for Wireless Communications Handbook*, M. Ibnkahla, Ed. Boca Raton, FL, USA: CRC Press, 2004.

[30] M. Steinbauer, A. F. Molisch, and E. Bonek, "The double-directional radio channel," *IEEE Antennas Propag. Mag.*, vol. 43, no. 4, pp. 51–63, Aug. 2001.

[31] A. F. Molisch, "Ultrawideband propagation channels-theory, measurement, and modeling," *IEEE Trans. Veh. Technol.*, vol. 54, no. 5, pp. 1528–1545, Sep. 2005.

[32] A. A. A. Glazunov, M. Gustafsson, and A. F. Molisch, "On the physical limitations of the interaction of a spherical aperture and a random field," *IEEE Trans. Antennas Propag.*, vol. 59, no. 1, pp. 119–128, Jan. 2011.

[33] Y. Miao, J.-I. Takada, K. Saito, K. Haneda, A. A. Glazunov, and Y. Gong, "Comparison of plane wave and spherical vector wave channel modeling for characterizing non-specular rough-surface wave scattering," *IEEE Antennas Wireless Propag. Lett.*, vol. 17, pp. 1847–1851, 2018.

[34] V. Kristem *et al.*, "3D MIMO outdoor-to-indoor propagation channel measurement," *IEEE Trans. Wireless Commun.*, vol. 16, no. 7, pp. 4600–4613, Jul. 2017.

[35] Y. Miao, K. Haneda, M. Kim, and J.-I. Takada, "Antenna de-embedding of radio propagation channel with truncated modes in the spherical vector wave domain," *IEEE Trans. Antennas Propag.*, vol. 63, no. 9, pp. 4100–4110, Sep. 2015.

[36] Y. Miao *et al.*, "Comparing channel emulation algorithms by using plane waves and spherical vector waves in multiprobe anechoic chamber setups," *IEEE Trans. Antennas Propag.*, vol. 67, no. 6, pp. 4091–4103, Jun. 2019.

[37] Y. Miao, K. Haneda, J.-I. Naganawa, M. Kim, and J.-I. Takada, "Measurement-based analysis and modeling of multimode channel behaviors in spherical vector wave domain," *IEEE Trans. Wireless Commun.*, vol. 19, no. 8, pp. 5345–5358, Aug. 2020.

[38] "Spatial channel model for multiple input multiple output (MIMO) simulations," 3rd Gener. Partnership Project(3GPP), Sophia Antipolis, France, Rep. 3GPP TR36.996, 2003.

[39] "Propagation data and prediction methods for the planning of indoor radio communication systems and radio local area networks in the frequency range 300 MHz to 450 GHz," ITU, Geneva, Switzerland, ITU-Recommendation P.1238-10, 2019.

[40] "Propagation data and prediction methods for the planning of short-range outdoor radio communication systems and radio local area networks in the frequency range 300 MHz to 100GHz," ITU, Geneva, Switzerland, ITU-Recommendation P.1411-10, 2019.

[41] D. Martin, M. Werner, and O. Afif, *Radio Technologies and Concepts for IMT-Advanced*. Chichester, U.K.: Wiley, 2010.

[42] P. Kyösti *et al.* "IST-4-027756 WINNER II D1.1.2 V1.2 WINNER II Channel Models." WINNER II Deliverable. Feb. 2008. [Online]. Available: https://www.cept.org/files/8339/winner2%20-%20final%20report.pdf

[43] "Multipath propagation and parameterization of its characteristics," ITU, Geneva, Switzerland, ITU-Recommendation P.1407-7 2019.

[44] E. M. Vitucci, F. Mani, V. Degli-Esposti, and C. Oestges, "Polarimetric properties of diffuse scattering from building walls: Experimental parameterization of a ray-tracing model," *IEEE Trans. Antennas Propag.*, vol. 60, no. 6, pp. 2961–2969, Jun. 2012.

[45] M. Käske and R. Thomä, "Maximum-likelihood based estimation of angular parameters of dense-multipath-components," in *Proc. 9th Eur. Conf. Antennas Propag. (EuCAP)*, 2015, pp. 1–6.

[46] B. Hanssens *et al.*, "Modeling the power angular profile of dense multipath components using multiple clusters," in *Proc. 12th Eur. Conf. Antennas Propag.*, 2018, pp. 1–5.

[47] A. Richter, J. Salmi, and V. Koivunen, "Signal processing perspectives to radio channel modelling," in *Proc. 2nd Eur. Conf. Antennas Propag. (EuCAP)*, 2007, pp. 1–6.

[48] F. Quitin, C. Oestges, F. Horlin, and P. De Doncker, "Diffuse multipath component characterization for indoor MIMO channels," in *Proc. 4th Eur. Conf. Antennas Propag. (EuCAP)*, 2010, pp. 1–5.

[49] F. Quitin, C. Oestges, F. Horlin, and P. De Doncker, "A polarized clustered channel model for indoor multiantenna systems at 3.6 GHz," *IEEE Trans. Veh. Technol.*, vol. 59, no. 8, pp. 3685–3693, Oct. 2010.

[50] F. Quitin, C. Oestges, F. Bellens, S. van Roy, F. Horlin, and P. De Doncker, "Extracting specular-diffuse clusters from MIMO channel measurements," in *Proc. IEEE 22nd Int. Symp. Pers. Indoor Mobile Radio Commun.*, 2011, pp. 940–944.

[51] N. Schneckenburger, T. Jost, D. Shutin, M. Walter, G. del Galdo, and U.-C. Fiebig, "Reflector localization for geometrical modeling the air–ground channel," *IEEE Trans. Veh. Technol.*, vol. 67, no. 9, pp. 7994–8008, Sep. 2018.

[52] N. Czink, F. Kaltenberger, Y. Zhou, L. Bernadó, T. Zemen, and X. Yin, "Low-complexity geometry-based modeling of diffuse scattering," in *Proc. 4th Eur. Conf. Antennas Propag.*, 2010, pp. 1–4.

[53] J. Karedal *et al.*, "A geometry-based stochastic MIMO model for vehicle-to-vehicle communications," *IEEE Trans. Wireless Commun.*, vol. 8, no. 7, pp. 3646–3657, Jul. 2009.

[54] J. Karedal *et al.*, "Measurement-based modeling of vehicle-to-vehicle MIMO channels," in *Proc. IEEE Int. Conf. Commun.*, 2009, pp. 1–6.

[55] J. Salmi *et al.*, "Incorporating diffuse scattering in geometry-based stochastic MIMO channel models," in *Proc. 4th Eur. Conf. Antennas Propag. (EuCAP)*, 2010, pp. 1–5.

[56] D. Didascalou, M. Dottling, N. Geng, and W. Wiesbeck, "An approach to include stochastic rough surface scattering into deterministic ray-optical wave propagation modeling," *IEEE Trans. Antennas Propag.*, vol. 51, no. 7, pp. 1508–1515, Jul. 2003.

[57] G. Gougeon, Y. Corre, and Y. Lostanlen, "Impact of the introduction of diffuse scattering on radio channel parameters in urban environments," in *Proc. 2nd Eur. Conf. Antennas Propag. (EuCAP)*, 2007, pp. 1–6.

[58] G. Gougeon, Y. Lostanlen, and L. Maviel, "Coupling a deterministic propagation model with diffuse scattering and urban furniture for small cells," in *Proc. 5th Eur. Conf. Antennas Propag. (EUCAP)*, 2011, pp. 3448–3452.

[59] F. Fuschini, H. El-Sallabi, V. Degli-Esposti, L. Vuokko, D. Guiducci, and P. Vainikainen, "Analysis of multipath propagation in urban environment through multidimensional measurements and advanced ray tracing simulation," *IEEE Trans. Antennas Propag.*, vol. 56, no. 3, pp. 848–857, Mar. 2008.

[60] E. M. Vitucci, F. Mani, V. Degli-Esposti, and C. Oestges, "A study on polarimetric properties of scattering from building walls," in *Proc. IEEE 72nd Veh. Technol. Conf. Fall*, 2010, pp. 1–5.

[61] V. Degli-Esposti, F. Fuschini, and E. M. Vitucci, "Implementation of a fast distributed scattering model for ray tracing prediction," in *Proc. 7th Eur. Conf. Antennas Propag. (EuCAP)*, 2013, pp. 3039–3042.

[62] E. M. Vitucci, F. Mani, C. Oestges, and V. Degli-Esposti, "Analysis and modeling of the polarization characteristics of diffuse scattering in indoor and outdoor radio propagation," in *Proc. ICECom*, 2013, pp. 1–5.

[63] F. Sheikh, D. Lessy, M. Alissa, and T. Kaiser, "A comparison study of non-specular diffuse scattering models at terahertz frequencies," in *Proc. 1st Int. Workshop Mobile THz Syst. (IWMTS)*, 2018, pp. 1–6.

[64] F. Sheikh, D. Lessy, and T. Kaiser, "A novel ray-tracing algorithm for non-specular diffuse scattered rays at terahertz frequencies," in *Proc. 1st Int. Workshop Mobile THz Syst. (IWMTS)*, 2018, pp. 1–6.

[65] J. S. Lu, H. L. Bertoni, and V. Degli-Esposti, "Scale model investigation of mechanisms for scattering from office buildings at 2 GHz," *IEEE Trans. Antennas Propag.*, vol. 62, no. 12, pp. 6435–6442, Dec. 2014.

[66] F. Fuschini, V. Degli-Esposti, and E. M. Vitucci, "A model for forward-diffuse scattering through a wall," in *Proc. 4th Eur. Conf. Antennas Propag.*, 2010, pp. 1–4.

[67] E. M. Vitucci, F. Mani, V. Degli-Esposti, and C. Oestges, "Dense multipath depolarization in outdoor and indoor radio transmissions," in *Proc. 31st URSI Gen. Assem. Sci. Symp. (URSI GASS)*, 2014, pp. 1–4.

[68] Y. Miao, Q. Gueuning, M. Gan, and C. Oestges, "Adding diffuse scattering correlation to effective roughness models in ray tracing," in *Proc. 11th Eur. Conf. Antennas Propag. (EUCAP)*, 2017, pp. 828–830.

[69] E. M. Vitucci, J. Chen, V. Degli-Esposti, J. S. Lu, H. L. Bertoni, and X. Yin, "Analyzing radio scattering caused by various building elements using millimeter-wave scale model measurements and ray tracing," *IEEE Trans. Antennas Propag.*, vol. 67, no. 1, pp. 665–669, Jan. 2019.

[70] S. Ju *et al.*, "Scattering mechanisms and modeling for terahertz wireless communications," in *Proc. IEEE Int. Conf. Commun. (ICC)*, 2019, pp. 1–7.

[71] M.-H. Ren *et al.*, "Diffuse scattering directive model parameterization method for construction materials at mmWave frequencies," *Int. J. Antennas Propag.*, vol. 2020, pp. 1–9, Dec. 2020.

[72] J. Pascual-Garcia, M.-T. Martinez-Ingles, J.-M. M. Garcia-Pardo, J. Rodriguez, and L. J. Llácer, "Using tuned diffuse scattering parameters in ray tracing channel modeling," in *Proc. 9th Eur. Conf. Antennas Propag. (EuCAP)*, 2015, pp. 1–4.

[73] H. Tian *et al.*, "Effect level based parameterization method for diffuse scattering models at millimeter-wave frequencies," *IEEE Access*, vol. 7, pp. 93286–93293, 2019.

[74] V. Degli-Esposti, "A diffuse scattering model for urban propagation prediction," *IEEE Trans. Antennas Propag.*, vol. 49, no. 7, pp. 1111–1113, Jul. 2001.

[75] V. Degli-Esposti, F. Fuschini, E. M. Vitucci, and G. Falciasecca, "Measurement and modelling of scattering from buildings," *IEEE Trans. Antennas Propag.*, vol. 55, no. 1, pp. 143–153, Jan. 2007.

[76] B. Antonescu, M. T. Moayyed, and S. Basagni, "Diffuse scattering models for mmWave V2X communications in urban scenarios," in *Proc. Int. Conf. Comput. Netw. Commun. (ICNC)*, 2019, pp. 923–929.

[77] B. Antonescu, M. T. Moayyed, and S. Basagni, "mmWave channel propagation modeling for V2X communication systems," in *Proc. IEEE 28th Annu. Int. Symp. Pers. Indoor Mobile Radio Commun. (PIMRC)*, 2017, pp. 1–6.

[78] J. Pascual-García, J. Molina-García-Pardo, M. Martínez-Inglès, J.-V. Rodríguez, and N. Saurín-Serrano, "On the importance of diffuse scattering model parameterization in indoor wireless channels at mm-wave frequencies," *IEEE Access*, vol. 4, pp. 688–701, 2016.

[79] J. Pascual-Garcia, M. Martinez-Ingles, J. Molina-Garcia-Pardo, J. Rodríguez, and V. Degli-Esposti, "Experimental parameterization of a diffuse scattering model at 60 GHz," in *Proc. IEEE-APS Topical Conf. Antennas Propag. Wireless Commun. (APWC)*, 2015, pp. 734–737.

[80] F. Mani and C. Oestges, "Evaluation of diffuse scattering contribution for delay spread and crosspolarization ratio prediction in an indoor scenario," in *Proc. 4th Eur. Conf. Antennas Propag.*, 2010, pp. 1–4.

[81] Y. Miao, Q. Gueuning, and C. Oestges, "Modeling the phase correlation of effective diffuse scattering from surfaces for radio propagation prediction with antennas at refined separation," *IEEE Trans. Antennas Propag.*, vol. 66, no. 3, pp. 1427–1435, Mar. 2018.

[82] L. Tian, V. Degli-Esposti, E. M. Vitucci, X. Yin, F. Mani, and S. X. Lu, "Semi-deterministic modeling of diffuse scattering component based on propagation graph theory," in *Proc. IEEE 25th Annu. Int. Symp. Pers. Indoor Mobile Radio Commun. (PIMRC)*, 2014, pp. 155–160.

[83] A. Velkers, "Investigating the coherence bandwidth and coherence distance of radio signals scattered from urban building point clouds using physical optics," B.S. thesis, Dept. Electr. Eng., Univ. Twente, Enschede, The Netherlands, 2020.

[84] J. Järveläinen, K. Haneda, M. Kyrö, V.-M. Kolmonen, J.-I. Takada, and H. Hagiwara, "60 GHz radio wave propagation prediction in a hospital environment using an accurate room structural model," in *Proc. Loughborough Antennas Propag. Conf. (LAPC)*, 2012, pp. 1–4.

[85] J. Järveläinen and K. Haneda, "Sixty gigahertz indoor radio wave propagation prediction method based on full scattering model," *Radio Sci.*, vol. 49, no. 4, pp. 293–305, 2014.

[86] J. Chen, X. Yin, L. Tian, and M.-D. Kim, "Millimeter-wave channel modeling based on a unified propagation graph theory," *IEEE Commun. Lett.*, vol. 21, no. 2, pp. 246–249, Feb. 2017.

[87] G. Steinböck *et al.*, "Hybrid model for reverberant indoor radio channels using rays and graphs," *IEEE Trans. Antennas Propag.*, vol. 64, no. 9, pp. 4036–4048, Sep. 2016.

[88] Y. Miao, T. Pedersen, M. Gan, E. Vinogradov, and C. Oestges, "Reverberant room-to-room radio channel prediction by using rays and graphs," *IEEE Trans. Antennas Propag.*, vol. 67, no. 1, pp. 484–494, Jan. 2019.

[89] W. Weichselberger, M. Herdin, H. Ozcelik, and E. Bonek, "A stochastic MIMO channel model with joint correlation of both link ends," *IEEE Trans. Wireless Commun.*, vol. 5, no. 1, pp. 90–100, Jan. 2006.

[90] C. B. Ribeiro, E. Ollila, and V. Koivunen, "Propagation parameter estimation in MIMO systems using mixture of angular distributions model," in *Proc. IEEE Int. Conf. Acoust. Speech Signal Process.*, vol. 4, 2005, pp. 885–888.

[91] K. V. Mardia, *Statistics of Directional Data*. London, U.K.: Academic, 1972.

[92] F. Quitin, C. Oestges, F. Horlin, and P. D. Doncker, "Clustered channel characterization for indoor polarized MIMO systems," in *Proc. IEEE Int. Symp. Pers. Indoor Mobile Radio Commun.*, 2009, pp. 1–5.

[93] K. Haneda, J.-I. Takada, and T. Kobayashi, "Cluster properties investigated from a series of ultrawideband double directional propagation measurements in home environments," *IEEE Trans. Antennas Propag.*, vol. 54, no. 12, pp. 3778–3788, Dec. 2006.

[94] J. Karedal, S. Wyne, P. Almers, F. Tufvesson, and A. F. Molisch, "A measurement-based statistical model for industrial ultra-wideband channels," *IEEE Trans. Wireless Commun.*, vol. 6, no. 8, pp. 3028–3037, Aug. 2007.

[95] M. Nieto-Vesperinas, *Scattering and Diffraction in Physical Optics*. New York, NY, USA: Wiley, 1991.

[96] J. A. Ogilvy, *Theory of Wave Scattering from Random Rough Surfaces*. Bristol, U.K.: Adam Higler, 1991.

[97] M. Ando, "Physical optics," in *Analysis Methods for Electromagnetic Wave Problems*, vol. 2, E. Yamashita, Eds. Norwood, MA, USA: Artech House, Inc., 1996, ch. 4.

[98] E. M. Vitucci, F. Mani, V. Degli-Esposti, and C. Oestges, "Study of a polarimetric model for diffuse scattering in urban environment," in *Proc. 6th Eur. Conf. Antennas Propag. (EUCAP)*, 2012, pp. 39–43.

[99] D. W. Matolak and Q. Wu, "Channel models for V2V communications: A comparison of different approaches," in *Proc. 5th Eur. Conf. Antennas Propag. (EUCAP)*, 2011, pp. 2891–2895.

[100] "Channel modeling and characterization," MiWEBA, Breitengüßbach, Germany, Rep. MiWEBA Deliverable D5.1, Jun. 2014. [Online]. Available: http://www.miweba.eu/wp-content/uploads/2014/07/MiWEBA

[101] R. J. Weiler *et al.*, "Quasi-deterministic millimeter-wave channel models in MiWEBA," *EURASIP J. Wireless Commun. Netw.*, vol. 2016, no. 1, pp. 1–16, 2016.

[102] C. Wang, J. Bian, J. Sun, W. Zhang, and M. Zhang, "A survey of 5G channel measurements and models," *IEEE Commun. Surveys Tuts.*, vol. 20, no. 4, pp. 3142–3168, 4th Quart., 2018.

[103] "METIS channel models," Mobile and Wireless Commun. Enablers Twenty-Twenty Inf. Soc. (METIS), London, U.K., Rep. Deliverable D1.4 ICT-317669-METIS/D1.4, Feb. 2015.

[104] I. Carton, W. Fan, P. Kyösti, and G. F. Pedersen, "Validation of 5G METIS map-based channel model at mmwave bands in indoor scenarios," in *Proc. 10th Eur. Conf. Antennas Propag. (EuCAP)*, 2016, pp. 1–5.

[105] "Study on channel model for frequencies from 0.5 to 100 GHz," 3rd Gener. Partnership Project, Sophia Antipolis, France, Rep. TR 38.901 version 16.1.0, Dec. 2019. [Online]. Available: https://portal.3gpp.org/desktopmodules/Specifications/SpecificationDetails.aspx?specificationId=3173

[106] R. Roy and T. Kailath, "ESPRIT-estimation of signal parameters via rotational invariance techniques," *IEEE Trans. Acoust., Speech, Signal Process.*, vol. 37, no. 7, pp. 984–995, Jul. 1989.

[107] R. Schmidt, "Multiple emitter location and signal parameter estimation," *IEEE Trans. Antennas Propag.*, vol. 34, no. 3, pp. 276–280, Mar. 1986.

[108] M. Feder and E. Weinstein, "Parameter estimation of superimposed signals using the EM algorithm," *IEEE Trans. Acoust., Speech, Signal Process.*, vol. 36, no. 4, pp. 477–489, Apr. 1988.

[109] B. H. Fleury, M. Tschudin, R. Heddergott, D. Dahlhaus, and K. I. Pedersen, "Channel parameter estimation in mobile radio environments using the SAGE algorithm," *IEEE J. Sel. Areas Commun.*, vol. 17, no. 3, pp. 434–450, Mar. 1999.

[110] R. M. Davis and R. L. Fante, "A maximum-likelihood beamspace processor for improved search and track," *IEEE Trans. Antennas Propag.*, vol. 49, no. 7, pp. 1043–1053, Jul. 2001.

[111] A. Richter and R. S. Thoma, "Joint maximum likelihood estimation of specular paths and distributed diffuse scattering," in *Proc. IEEE 61st Veh. Technol. Conf.*, vol. 1, 2005, pp. 11–15.

[112] B. Hanssens *et al.*, "An extension of the RiMAX multipath estimation algorithm for ultra-wideband channel modeling," *EURASIP J. Wireless Commun. Netw.*, vol. 2018, no. 1, pp. 1–22, 2018.

[113] W. Wang, T. Jost, and A. Dammann, "Estimation and modelling of NLoS time-variant multipath for localization channel model in mobile radios," in *Proc. IEEE Global Commun. Conf. (GLOBECOM)*, Miami, FL, USA, Dec. 2010, pp. 1–6.

[114] J. Poutanen, J. Salmi, K. Haneda, V.-M. Kolmonen, F. Tufvesson, and P. Vainikainen, "Propagation characteristics of dense multipath components," *IEEE Antennas Wireless Propag. Lett.*, vol. 9, pp. 791–794, 2010.

[115] V. Degli-Esposti *et al.*, "Ray-tracing-based mm-wave beamforming assessment," *IEEE Access*, vol. 2, pp. 1314–1325, 2014.

[116] M. Landmann, "Limitations of experimental channel characterisation," Ph.D. dissertation, Dept. Technische Universität Ilmenau, Tu Ilmenau, Ilmenau, Germany, 2008.

[117] E. Tanghe *et al.*, "Dense multipath component polarization and wall attenuation at 1.35 GHz in an office environment," in *Proc. 12th Eur. Conf. Antennas Propag. (EuCAP)*, 2018, pp. 1–5.

[118] K. Saito, J.-I. Takada, and M. Kim, "Dense multipath component parameter estimation in 11GHz-band indoor environment," in *Proc. IEEE 27th Annu. Int. Symp. Pers. Indoor Mobile Radio Commun. (PIMRC)*, 2016, pp. 1–6.

[119] K. Saito, J. Takada, and M. Kim, "Characteristics evaluation of dense multipath component in 11GHz-band indoor environment," in *Proc. 10th Eur. Conf. Antennas Propag. (EuCAP)*, 2016, pp. 1–3.

[120] A. Richter, M. Enescu, and V. Koivunen, "State-space approach to propagation path parameter estimation and tracking," in *Proc. IEEE 6th Workshop Signal Process. Adv. Wireless Commun.*, 2005, pp. 510–514.

[121] J. Salmi, A. Richter, M. Enescu, P. Vainikainen, and V. Koivunen, "Propagation parameter tracking using variable state dimension Kalman filter," in *Proc. IEEE 63rd Veh. Technol. Conf.*, vol. 6, 2006, pp. 2757–2761.

[122] N. Czink, A. Richter, E. Bonek, J.-P. Nuutinen, and J. Ylitalo, "Including diffuse multipath parameters in MIMO channel models," in *Proc. IEEE 66th Veh. Technol. Conf.*, 2007, pp. 874–878.

[123] S. Hinteregger, E. Leitinger, and K. Witrisal, "Bayesian multipath channel estimation considering dense multipath," in *Proc. Workshop Depend. Wireless Commun. Localization IoT COST IRACON*, Graz, Austria, 2017, pp. 1–4.

[124] J. Li, B. Ai, R. He, M. Yang, and Z. Zhong, "On modeling of dense multipath component for indoor massive MIMO channels," *IEEE Antennas Wireless Propag. Lett.*, vol. 18, pp. 526–530, 2019.

[125] A. Bamba *et al.*, "Experimental investigation of the characteristics of the electromagnetic reverberation in the UWB bands," in *Proc. IEEE Antennas Propag. Soc. Int. Symp. (APSURSI)*, 2014, pp. 1181–1182.

[126] A. Bamba *et al.*, "Experimental investigation of electromagnetic reverberation characteristics as a function of UWB frequencies," *IEEE Antennas Wireless Propag. Lett.*, vol. 14, pp. 859–862, 2015.

[127] A. Richter, J. Salmi, and V. Koivunen, "Distributed scattering in radio channels and its contribution to MIMO channel capacity," in *Proc. 1st Eur. Conf. Antennas Propag.*, 2006, pp. 1–7.

[128] A. Richter, "The contribution of distributed scattering in radio channels to channel capacity: Estimation and modeling," in *Proc. 40th Asilomar Conf. Signals Syst. Comput.*, 2006, pp. 951–955.

[129] B. Hanssens, "Indoor ultra-wideband channel modeling and localization using multipath estimation algorithms," Ph.D. dissertation, Dept. Inf. Technol., Ghent Univ., Ghent, Belgium, 2018.

[130] B. Hanssens *et al.*, "Measurement-based analysis of dense multipath components in a large industrial warehouse," in *Proc. 12th Eur. Conf. Antennas Propag. (EuCAP)*, 2018, pp. 1–5.

[131] D. P. Gaillot *et al.*, "Polarization properties of specular and dense multipath components in a large industrial hall," *IEEE Trans. Antennas Propag.*, vol. 63, no. 7, pp. 3219–3228, Jul. 2015.

[132] D. P. Gaillot *et al.*, "Polarization properties of specular and dense multipath components in a large industrial hall," in *Proc. 31st URSI Gen. Assem. Sci. Symp. (URSI GASS)*, 2014, pp. 1–4.

[133] M.-T. Martinez-Ingles, D. P. Gaillot, J. Pascual-Garcia, J.-M. Molina-Garcia-Pardo, M. Lienard, and J.-V. Rodríguez, "Deterministic and experimental indoor mmW channel modeling," *IEEE Antennas Wireless Propag. Lett.*, vol. 13, pp. 1047–1050, 2014.

[134] W. A. T. Kotterman, M. Landmann, G. Sommerkorn, and R. Thomä, "On diffuse and non-resolved multipath components in directional channel characterisation," in *Proc. Gen. Assem. URSI*, New Delhi, India, Oct. 2005, pp. 1–4.

[135] F. Quitin, C. Oestges, F. Bellens, S. Van Roy, F. Horlin, and P. De Doncker, "Model parametrization and validation for specular-diffuse clustered channel models," *IEEE Trans. Antennas Propag.*, vol. 60, no. 8, pp. 4019–4022, Aug. 2012.

[136] A. A. Goulianos *et al.*, "Measurements and characterisation of surface scattering at 60 GHz," in *Proc. IEEE 86th Veh. Technol. Conf. (VTC-Fall)*, 2017, pp. 1–5.

[137] S. Jiang, X. Zhang, W. Wang, M. Yang, and R. He, "Measurement and diffuse multipath analysis of V2V propagation channel at 5.9 GHz in tunnel area," in *Proc. 14th Eur. Conf. Antennas Propag. (EuCAP)*, 2020, pp. 1–5.

[138] K. Haneda, J. Järveläinen, A. Karttunen, M. Kyrö, and J. Putkonen, "A statistical spatio-temporal radio channel model for large indoor environments at 60 and 70 GHz," *IEEE Trans. Antennas Propag.*, vol. 63, no. 6, pp. 2694–2704, Jun. 2015.

[139] D. Solomitckii *et al.*, "Characterizing the impact of diffuse scattering in urban millimeter-wave deployments," *IEEE Wireless Commun. Lett.*, vol. 5, no. 4, pp. 432–435, Aug. 2016.

[140] T. Abbas, J. Karedal, F. Tufvesson, A. Paier, L. Bernado, and A. F. Molisch, "Directional analysis of vehicle-to-vehicle propagation channels," in *Proc. IEEE 73rd Veh. Technol. Conf. (VTC Spring)*, 2011, pp. 1–5.

[141] C. Gustafson, F. Tufvesson, S. Wyne, K. Haneda, and A. F. Molisch, "Directional analysis of measured 60 GHz indoor radio channels using SAGE," in *Proc. IEEE 73rd Veh. Technol. Conf. (VTC Spring)*, 2011, pp. 1–5.

[142] D. Porrat, "The diffuse multipath component and multipath component visibility," in *Proc. 5th Eur. Conf. Antennas Propag. (EUCAP)*, 2011, pp. 3774–3777.

[143] M. Käske and R. S. Thomä, "Analysis of angular parameters of dense multipath components in an urban macro-cell scenario," in *Proc. 5th Eur. Conf. Antennas Propag. (EUCAP)*, 2011, pp. 3429–3433.

[144] B. Hanssens *et al.*, "Measurement-based analysis of specular and dense multipath components at 94 GHz in an indoor environment," *IET Microw. Antennas Propag.*, vol. 12, no. 4, pp. 509–515, 2018.

[145] M. Landmann, K. Sivasondhivat , J.-I. Takada, I. Ida, and R. Thomä, "Polarization behavior of discrete multipath and diffuse scattering in urban environments at 4.5 GHz," *EURASIP J. Wireless Commun. Netw.*, vol. 2007, no. 1, pp. 1–15, 2007.

[146] J. Ø. Nielsen, J. B. Andersen, G. F. Pedersen, and M. Pelosi, "On polarization and frequency dependence of diffuse indoor propagation," in *Proc. IEEE Veh. Technol. Conf. (VTC-Fall)*, 2011, pp. 1–5.

[147] Y. Zhou, X. Yin, N. Czink, T. Zemen, A. Guo, and F. Liu, "Evaluation of doppler-delay properties of diffuse components in vehicular propagation channels," in *Proc. 2nd IEEE Int. Conf. Wireless Access Veh. Environ.*, Shanghai, China, Dec. 2009, pp. 1–6.

[148] D. Solomitckii *et al.*, "Ray-based evaluation of dual-polarized MIMO in (ultra-)dense millimeter-wave urban deployments," in *Proc. IEEE 87th Veh. Technol. Conf. (VTC Spring)*, 2018, pp. 1–7.

[149] G. Wunder, H. Boche, T. Strohmer, and P. Jung, "Sparse signal processing concepts for efficient 5G system design," *IEEE Access*, vol. 3, pp. 195–208, 2015.

[150] Z. Yan, M. Herdin, A. M. Sayeed, and E. Bonek, "Experimental study of MIMO channel statistics and capacity via virtual channel representation," Dept. Electron. Commun. Eng., Univ. Wisconsin-Madison, Madison, WI, USA, Rep., Feb. 2007.

[151] S. Sun, T. S. Rappaport, M. Shafi, P. Tang, J. Zhang, and P. J. Smith, "Propagation models and performance evaluation for 5G millimeter-wave bands," *IEEE Trans. Veh. Technol.*, vol. 67, no. 9, pp. 8422–8439, Sep. 2018.

[152] S. Nguyen, "Compressive sensing for multi-channel and large-scale MIMO networks," Ph.D. dissertation, Dept. Electr. Comput. Eng., Concordia Univ., Montreal, QC, Canada, 2013.

[153] H. Al-Salihi and M. R. Nakhai, "Bayesian compressed sensing-based channel estimation for massive MIMO systems," in *Proc. Eur. Conf. Netw. Commun. (EuCNC)*, 2016, pp. 360–364.

[154] X. Cheng, M. Wang, and Y. L. Guan, "Ultrawideband channel estimation: A Bayesian compressive sensing strategy based on statistical sparsity," *IEEE Trans. Veh. Technol.*, vol. 64, no. 5, pp. 1819–1832, May 2015.

[155] R. Mateur, M. Hajjaj, and R. Bouallegue, "Sparsity adaptive subspace pursuit based channel estimation algorithm for OFDM based massive MIMO systems," in *Proc. Int. Conf. Internet Things Embedded Syst. Commun. (IINTEC)*, 2017, pp. 85–88.

[156] N. Michelusi, U. Mitra, A. F. Molisch, and M. Zorzi, "UWB sparse/diffuse channels, part I: Channel models and Bayesian estimators," *IEEE Trans. Signal Process.*, vol. 60, no. 10, pp. 5307–5319, Oct. 2012.

[157] N. Michelusi, U. Mitra, A. F. Molisch, and M. Zorzi, "UWB sparse/diffuse channels, part II: Estimator analysis and practical channels," *IEEE Trans. Signal Process.*, vol. 60, no. 10, pp. 5320–5333, Oct. 2012.

[158] A. H. Khanshan and H. Amindavar, "Performance evaluation of two-dimensional interpolations on OFDM channel estimation," in *Proc. Aust. Telecommun. Netw. Appl. Conf.*, 2007, pp. 460–464.

[159] H. Zhang, B. Ai, W. Xu, L. Xu, and S. Cui, "Multi-antenna channel interpolation via tucker decomposed extreme learning machine," *IEEE Trans. Veh. Technol.*, vol. 68, no. 7, pp. 7160–7163, Jul. 2019.

[160] A. Osinsky, A. Ivanov, and D. Yarotsky, "Bayesian approach to channel interpolation in massive MIMO receiver," *IEEE Commun. Lett.*, vol. 24, no. 12, pp. 2751–2755, Dec. 2020.

[161] P. Wu, X. Chen, and S. Qiu, "Performance comparison of ICM channel estimation with interpolations in OFDM/OQAM system," in *Proc. 3rd IEEE Int. Conf. Comput. Commun. (ICCC)*, 2017, pp. 147–151.

[162] Y. Chai, F. Hu, and L. Jin, "A novel time interpolation channel estimation for IEEE802.11ac system," in *Proc. 6th IEEE Int. Conf. Softw. Eng. Serv. Sci. (ICSESS)*, 2015, pp. 722–725.

[163] C. Rezgui and K. Grayaa, "An enhanced channel estimation technique with adaptive pilot spacing for OFDM system," in *Proc. Int. Symp. Netw. Comput. Commun. (ISNCC)*, 2016, pp. 1–4.

[164] M. D. Larsen, A. L. Swindlehurst, and T. Svantesson, "Performance bounds for MIMO-OFDM channel estimation," *IEEE Trans. Signal Process.*, vol. 57, no. 5, pp. 1901–1916, May 2009.

[165] F. Rottenberg, T. Choi, P. Luo, C. J. Zhang, and A. F. Molisch, "Performance analysis of channel extrapolation in FDD massive MIMO systems," *IEEE Trans. Wireless Commun.*, vol. 19, no. 4, pp. 2728–2741, Apr. 2020.

[166] N. Jalden, H. Asplund, and J. Medbo, "Channel extrapolation based on wideband MIMO measurements," in *Proc. 6th Eur. Conf. Antennas Propag. (EUCAP)*, 2012, pp. 442–446.

[167] Y. Miao and J. Takada, "Pattern reconstruction for deviated AUT in spherical measurement by using spherical waves," *IEICE Trans. Commun.*, vol. 97, no. 1, pp. 105–113, 2014.

[168] T. G. Vasiliadis, A. G. Dimitriou, and G. D. Sergiadis, "A novel technique for the approximation of 3-D antenna radiation patterns," *IEEE Trans. Antennas Propag.*, vol. 53, no. 7, pp. 2212–2219, Jul. 2005.

[169] D.-H. Yun, S.-H. Moon, and D.-S. Han, "Adaptive array algorithm using spatial interpolation for the cancellation of coherent interferences," in *Proc. IEEE Int. Conf. Commun. Conf. Rec.*, vol. 3, 2001, pp. 915–919.

[170] T. Choi *et al.*, "Channel extrapolation for FDD massive MIMO: Procedure and experimental results," in *Proc. IEEE 90th Veh. Technol. Conf. (VTC-Fall)*, 2019, pp. 1–6.

[171] C. De Lima *et al.*, "Convergent communication, sensing and localization in 6G Systems: An overview of technologies, opportunities and challenges," *IEEE Access*, vol. 9, pp. 26902–26925, 2021.

[172] A. Bourdoux *et al.*, "6G white paper on localization and sensing," 2020, *arXiv:2006.01779*.

[173] F. Wen, J. Kulmer, K. Witrisal, and H. Wymeersch, "5G positioning and mapping with diffuse multipath," *IEEE Trans. Wireless Commun.*, vol. 20, no. 2, pp. 1164–1174, Feb. 2021.

[174] F. Wen and H. Wymeersch, "5G synchronization, positioning, and mapping from diffuse multipath," *IEEE Wireless Commun. Lett.*, vol. 10, no. 1, pp. 43–47, Jan. 2021.

[175] Y. Ge *et al.*, "5G SLAM using the clustering and assignment approach with diffuse multipath," *Sensors*, vol. 20, no. 16, pp. 4656–4687, 2020.

[176] Y. Ge, H. Kim, F. Wen, L. Svensson, S. Kim, and H. Wymeersch, "Exploiting diffuse multipath in 5G SLAM," 2020, *arXiv:2006.15603*.
[177] H. Alidoustaghdam, A. Kokkeler, and Y. Miao, "Contact-free human posture estimation: An analysis of the influence of mmWave array polarization," in *Proc. Gen. Assem. Sci. Symp. Int. Union Radio Sci. (URSI GASS)*, 2021, pp. 1–4.
[178] Y. Miao *et al.*, "Measurement-based feasibility exploration on detecting and localizing multiple humans using MIMO radio channel properties," *IEEE Access*, vol. 8, pp. 3738–3750, 2020.
[179] M. Cheffena, "Physical-statistical channel model for signal effect by moving human bodies," *EURASIP J. Wireless Commun. Netw.*, vol. 2012, no. 1, pp. 1–13, 2012.
[180] M. Yokota, T. Ikegamai, Y. Ohta, and T. Fujii, "Numerical examination of EM wave shadowing by human body," in *Proc. 4th Eur. Conf. Antennas Propag.*, 2010, pp. 1–4.
[181] A. Bamba, E. Tanghe, W. Joseph, G. Vermeeren, D. Plets, and L. Martens, "Theory for exposure prediction in an indoor environment due to UWB systems," in *Proc. IEEE Int. Symp. Antennas Propag.*, 2012, pp. 1–2.
[182] S. Chang, M. Wolf, and J. W. Burdick, "Human detection and tracking via ultra-wideband (UWB) radar," in *Proc. IEEE Int. Conf. Robot. Autom.*, 2010, pp. 452–457.
[183] Y. Yang, D. Feng, X. Wang, and S. Xiao, "Effects of K distributed sea clutter and multipath on radar detection of low altitude sea surface targets," *IET Radar Sonar Navig.*, vol. 8, no. 7, pp. 757–766, 2014.
[184] Y. Xia, Z. Song, Z. Lu, and Q. Fu, "Target detection in low grazing angle with adaptive OFDM radar," *Progr. Electromagn. Res. M*, vol. 46, pp. 101–112, Jan. 2016.
[185] Y. Jin, J. M. F. Moura, N. O'Donoughue, and J. Harley, "Single antenna time reversal detection of moving target," in *Proc. IEEE Int. Conf. Acoust. Speech Signal Process.*, 2010, pp. 3558–3561.
[186] H. T. Hayvaci, A. D. Maio, and D. Erricolo, "Improved detection probability of a radar target in the presence of multipath with prior knowledge of the environment," *IET Radar Sonar Navig.*, vol. 7, no. 1, pp. 36–46, 2013.
[187] G. Yu, D. Zhao, and S. Piao, "Target detection method using multi-path information in an underwater waveguide environment," *IET Radar Sonar Navig.*, vol. 14, no. 2, pp. 226–232, 2020.
[188] A. Aubry, A. De Maio, G. Foglia, and D. Orlando, "Diffuse multipath exploitation for adaptive radar detection," *IEEE Trans. Signal Process.*, vol. 63, no. 5, pp. 1268–1281, Mar. 2015.
[189] Y. Rong, A. Aubry, A. De Maio, and M. Tang, "Diffuse multipath exploitation for adaptive detection of range distributed targets," *IEEE Trans. Signal Process.*, vol. 68, pp. 1197–1212, 2020.
[190] Z. Zhang *et al.*, "6G wireless networks: Vision, requirements, architecture, and key technologies," *IEEE Veh. Technol. Mag.*, vol. 14, no. 3, pp. 28–41, Sep. 2019.
[191] H. Tataria, M. Shafi, A. F. Molisch, M. Dohler, H. Sjöland, and F. Tufvesson, "6G wireless systems: Vision, requirements, challenges, insights, and opportunities," *Proc. IEEE*, vol. 109, no. 7, pp. 1166–1199, Jul. 2021.
[192] W. Fan, I. Carton, J. Ø. Nielsen, K. Olesen, and G. F. Pedersen, "Measured wideband characteristics of indoor channels at centimetric and millimetric bands," *EURASIP J. Wireless Commun. Netw.*, vol. 2016, no. 58, pp. 1–14, 2016.
[193] Y. Miao *et al.*, "Investigating correlation of rough surface diffuse scattering in frequency domain," in *Proc. 13th Eur. Conf. Antennas Propag. (EuCAP)*, 2019, pp. 1–3.
[194] R. Sun, "Dual-band non-stationary channel modeling for the air-ground channel," Ph.D. dissertation, Dept. Electr. Eng., Univ. South Carolina, Columbia, SC, USA, 2015.
[195] A. Bamba, W. Joseph, E. Tanghe, G. Vermeeren, and L. Martens, "Circuit model for diffuse multipath and electromagnetic absorption prediction in rooms," *IEEE Trans. Antennas Propag.*, vol. 61, no. 6, pp. 3292–3301, Jun. 2013.